Bulletin of the

Seismological Society of America

Vol. 55 April, 1965 No. 2

A PROCEDURE FOR SOURCE STUDIES FROM SPECTRUMS OF LONG-PERIOD SEISMIC BODY WAVES

By Ari Ben-Menahem, Stewart W. Smith, and Ta-Liang Teng

ABSTRACT

The well-known first motion method of Nakano and Byerly is extended, generalized and combined with recent new ideas in body wave theory in order to set up a routine procedure for extracting source parameters from spectral analysis of isolated P and S pulses recorded at a net of standardized stations around a non-shallow source.

The method consists of compensating the observed spectrums for instrumental and propagational effects. A combined study of the resulting radiation patterns, initial phases, and the initial amplitudes will render information regarding the spatial and temporal nature of deep and intermediate earthquake sources as seen through the spectral window of 10–100 seconds. The shorter periods can be used for source studies only if an accurate station correction is available.

Introduction

Early observations on the existence of certain regularities in the distribution of the sense of first-motions led seismologists to the development of a technique by which first-motion data was interpreted in terms of the orientation of an equivalent force system at the source. Numerous earthquakes have been analyzed by various investigators since Byerly (1926) first applied Nakano's theory (1923) to the Montana earthquake of June 28, 1925. The mere fact that the initial motions from many earthquakes could be fitted with a reasonable amount of scatter, to Nakano's simple model, indicates that seismic sources can be classified according to certain categories and hence can be expressed in terms of some parameters which may vary from one earthquake to another. However, in order to derive these parameters from the seismogram one must consider not only the initial motion but rather the entire spectrum of the pulse.

Recent investigations by Brune (1964a, b) and Ben-Menahem (1964a) have clarified the relationships between isolated body wave pulses and the total displacement field which the seismic source induces in the spherical earth. These studies show that each ray arrival carries with it source information which can be retrieved by the same technique used previously for the analysis of long period surface waves. Thus, it becomes unnecessary to go through the formidable process of the numerical solution of Lamb's problem for a layered spherical earth if one wishes to study only very particular portion of the total field.

Assuming the validity of ray-theory and considering the earth's mantle as a linear system we may look on the spectrums of P and S pulses at the far field as a product of a number of factors which depend on the history of the signal. That is to

say, we may trace the ray back from the station to the source and correct, one by one, for all the factors which took part in shaping the waveform of the signal. In the present paper we shall restrict our discussion to non-shallow shocks which we shall define by the condition p^*P-$P > 45$ sec ($h > 300$ km) where p^*P is the first reflection arrival from either the free surface or the bottom of the crust at the source.

1. *Removal of Crustal Distortion*

Haskell (1960) carried out the calculations for the response of an arbitrary layered elastic medium to incident plane harmonic waves of P and SV types using the layer matrix technique which he had outlined earlier. Neglecting the curvature of the wave-fronts, we have used here Haskell's formulation to calculate the amplitude and phase of horizontal and vertical components of the surface motion due to plane waves incident at the base of a stack of layers. This calculation was made for a number of well documented crustal models in an attempt to determine if the distortion of the body wave signal by near surface layering is significant enough to be considered when making source mechanism studies. In order to compare the forms of P and S waves at different stations, the frequency dependent transmission coefficients for each layered model were multiplied by the frequency response of a critically damped long period seismograph of the type used in the USCGS Worldwide standard stations (30 second pendulum, 100 second galvanometer). Then, using a synthesis technique described by Aki (1960), a plane wave, with a delta function time dependence, was simulated at the base of a stack of layers, and the resulting transient pulse in both horizontal and vertical motion was calculated at the surface. As a check on the quality of the frequency synthesis, a model was used where all of the layer parameters were the same, thus there should be no change in the pulse form due to the layered medium. The resulting surface motion was rectilinearly polarized and closely approximated the impulse response of the seismograph system.

A machine output for a particular case is shown in Table 1. A plane wave of unit amplitude is incident at an angle of 23.64° (apparent velocity of $C = 20$ km/sec) below a Gutenberg CEGH Upper mantle model. The columns from left are: Frequency F (cyc/sec), period T (sec), phase difference (deg) between vertical and horizontal spectral ground motion, horizontal surface ground motion, vertical surface ground motion, phase of vertical ground motion minus $\pi/2$ (parts of circle). The last four columns from the right give the spectrums of horizontal and vertical seismogram traces written by a standard seismograph system (30–100) with peak magnification of 2.2. Phase delays are in seconds.

The crustal structures which were used in the various examples are given in Table 2. The last row in each structure refers to the half-space below the layers. The structures were taken from Healy (1963), Roller and Healy (1963), Jackson, et al (1963), Aki and Press (1961), and Aki (1961).

Crustal amplitude responses for these models are shown in Figures 1–5. These results show very clearly that the different geologic provinces are significant even for periods as long as 10 seconds. This agrees with former results of Phinney (1964). It is thus evident that the shorter periods cannot be used for source studies unless an accurate station correction is applied.

Phase delays vs. period are exhibited for a number of models in Figures 6 and 7.

The combined effect of the layering and the seismograph system (30–100) is shown in Figure 8 for the Gutenberg CEGH model together with the response of the 30–100 seismograph system. The function $\{\text{amp}\ (\omega)e^{iPh(\omega)}\}$ (such as is shown in Fig. 8) may be considered as an inverse filter to be applied to the observed spec-

TABLE 1

SPECTRAL RESPONSE OF A LAYERED CRUST MODEL AND A 30–100 PRESS-EWING SEISMOGRAPH SYSTEM TO A PLANE DILATATIONAL BODY WAVE OF UNIT AMPLITUDE

6 LAYERS	ALPHA	BETA	RHO	MU	H
PACIFIC 6EGH GUTENBERG (LOW VEL LAYER)					
	6.0300	3.5300	2.7800	34.6413	22.0000
	6.7000	4.4000	3.0000	60.4803	15.0000
	8.0000	4.6000	3.3300	70.4629	13.0000
	7.8400	4.4300	3.3500	67.5363	25.0000
	7.8400	4.3800	3.3700	64.6514	50.0000
	8.0200	4.3800	3.4200	65.6106	0.

PACIFIC 6EGH GUTENBERG (LOW VEL LAYER)

INCIDENT P WAVES. C = 20.0000. THN = 23.6407. THO = 17.5477.

F	T	PHI	/X/	/Z/	PHASE	AMP-H	PH-H-sec	AMP-V	PH-V-sec
0.	0.	0.	0.	0.	0.	0.	0.	0.	0.
0.0062	160.0000	0.9368	0.9944	1.8563	0.6644	0.217286	11.173537	0.450963	11.589882
0.0125	80.0000	0.7514	0.9692	1.9537	0.5749	0.927673	25.797839	1.876006	25.964823
0.0187	53.3333	0.3439	1.0860	2.0641	0.4810	1.724967	28.012490	3.278681	28.063440
0.0250	40.0000	355.1303	1.2515	2.1784	0.3864	2.472551	28.433865	4.303966	27.892789
0.0312	32.0000	345.4983	1.3314	2.3603	0.2902	2.877215	28.521070	5.100830	27.231145
0.0375	26.6667	340.1458	1.3017	2.5901	0.1867	2.881327	1.445276	5.732576	26.641564
0.0437	22.8571	337.9977	1.2527	2.7837	0.0759	2.740122	4.718410	6.089538	3.321442
0.0500	20.0000	339.0315	1.1226	2.8526	0.9599	2.378712	6.967492	6.044507	5.802574
0.0562	17.7778	344.7882	1.0056	2.7317	0.8458	2.041320	8.368377	5.545111	7.607175
0.0625	16.0000	348.2662	0.9495	2.6485	0.7406	1.835513	9.368714	4.926395	8.847210
0.0687	14.5455	350.3686	0.9085	2.4231	0.6406	1.667485	10.131025	4.447716	9.741879
0.0750	13.3333	352.0267	0.9060	2.3250	0.5476	1.577503	10.749888	4.047969	10.454580
0.0812	12.3077	350.4858	0.8907	2.2039	0.4423	1.471124	11.338482	3.640052	11.013210
0.0875	11.4286	348.4302	0.8409	2.0904	0.3491	1.318445	0.353440	3.277655	11.414716
0.0937	10.6667	346.6999	0.7985	2.0450	0.2604	1.189927	1.428726	3.047340	1.034649
0.1000	10.0000	347.9394	0.7632	2.0913	0.1710	1.082410	2.283316	2.965975	1.948300
0.1062	9.4118	354.2192	0.8128	2.1862	0.0701	1.098637	2.949151	2.655131	2.798020
0.1125	8.8889	355.0304	0.9704	2.2522	0.9770	1.252199	3.705720	2.906166	3.583014
0.1187	8.4211	348.4910	1.0933	2.2924	0.8787	1.348680	4.542586	2.827886	4.273369
0.1250	8.0000	340.2395	1.1756	2.3474	0.7815	1.388555	5.320465	2.772640	4.881344
0.1312	7.6190	327.5914	1.2353	2.4646	0.6841	1.398708	6.114682	2.791352	5.428785
0.1375	7.2727	312.8868	1.1462	2.6500	0.5786	1.246455	6.934147	2.881837	5.982366
0.1437	6.9565	301.4110	0.8718	2.6938	0.4639	0.911587	0.775050	2.816656	6.549419
0.1500	6.6667	295.5934	0.5346	2.5364	0.3540	0.538134	1.560916	2.653205	0.368201
0.1562	6.4000	300.1310	0.2692	2.3712	0.2544	0.261203	2.078088	2.300762	1.013751
0.1625	6.1538	351.1863	0.1068	2.2927	0.1592	0.100007	1.731162	2.146736	1.580500
0.1687	5.9259	55.5392	0.2527	2.2730	0.0676	0.228590	1.198189	2.056059	2.112415
0.1750	5.7143	56.1664	0.4953	2.2430	0.9636	0.433234	1.727396	1.962061	2.618927
0.1812	5.5172	47.2762	0.7115	2.1769	0.8662	0.602455	2.356061	1.843338	3.080600
0.1875	5.3333	36.5554	0.8777	2.1243	0.7729	0.720106	2.946933	1.742921	3.498494
0.1937	5.1613	24.9218	1.0326	2.1189	0.6816	0.821686	3.501956	1.686046	3.859258
0.2000	5.0000	9.6613	1.1315	2.1660	0.5917	0.873911	4.065200	1.672907	4.199385
0.2062	4.8485	356.2752	1.1059	2.3195	0.4993	0.829690	4.580010	1.740237	4.529845
0.2125	4.7059	349.8779	1.0366	2.5128	0.3982	0.756049	0.307651	1.832750	0.175336
0.2187	4.5714	346.2140	0.9663	2.6614	0.2926	0.685672	0.836634	1.888453	0.661573
0.2250	4.4444	344.1006	0.8644	2.7875	0.1840	0.597127	1.329991	1.925571	1.133702
0.2312	4.3243	345.5961	0.7317	2.8370	0.0700	0.492400	1.776012	1.909219	1.602872
0.2375	4.2105	352.4171	0.5692	2.7027	0.9555	0.373422	2.137958	1.773039	2.049269
0.2437	4.1026	7.5379	0.4555	2.4586	0.8500	0.291435	2.349598	1.573236	2.435499
0.2500	4.0000	24.9853	0.4393	2.2699	0.7542	0.274344	2.490220	1.417579	2.763390

trums of body waves from non-shallow shocks. The application of such a filter to periods above 10 sec virtually projects the body wave pulse below the crust.

Figures 9 and 10 show the combined impulse response of various layered structures and a long period seismograph to incident S and P waves respectively. The synthesis was performed using 80 frequency bands of equal width between 0.0 and 0.5 cps, and the time function was computed at intervals of 1 second. The general shape of the P wave is predominantly controlled by the seismograph characteristics;

however, the peak amplitude and some of the shorter period oscillations are strongly affected by the layered structure. This is as expected, the predominant distortion of the waves that occurs for wavelengths comparable with the layer thickness.

The S wave pulse distortion shown in Figure 10, appears to be somewhat more complicated than the P waves shown in Figure 9. This is because some of the converted waves arrive before the direct S wave. The first arrival visible in most cases is converted from S to P at the base of the stack of layers and travels through the

TABLE 2

CRUSTAL STRUCTURES OF SOME GEOLOGIC PROVINCES IN NORTH AMERICA AND THE PACIFIC

	ALPHA	BETA	RHO	MU	H
SANTA MONICA-SAN FRANCISCO HEALY					
	6.1000	3.3800	2.8500	32.5595	27.0000
	8.2000	4.5400	3.4000	70.0794	-0.
SANTA MONICA-LAKE MEAD ROLLER AND HEALY					
	3.0000	1.6600	2.3500	6.4757	2.9000
	6.3000	3.4800	2.8500	34.5146	28.4000
	7.8000	4.3200	3.2800	61.2127	-0.
EASTERN COLORADO JACKSON ET AL					
	2.9000	1.6000	2.3000	5.8880	0.6000
	4.8000	2.6600	2.6500	18.7503	0.4000
	5.2000	2.8800	2.6700	22.1460	1.3000
	5.8000	3.2100	2.8000	28.8515	9.9000
	6.1000	3.3800	2.8500	32.5595	15.5000
	6.7000	3.7100	3.0500	41.9805	20.0000
	8.0000	4.4300	3.3500	65.7434	-0.
CONTINENT GE PRESS					
	6.0300	3.5300	2.7800	34.6413	22.0000
	6.7000	4.4900	3.0000	60.4803	15.0000
	8.0000	4.6000	3.3300	70.4628	-0.
JAPAN GEJ AKI					
	5.7000	3.3300	2.7800	30.8271	22.0000
	6.3300	3.5900	3.0000	38.6643	15.0000
	7.5200	4.3500	3.3300	63.0119	-0.
PACIFIC GEGH GUTENBERG (LOW VEL LAYER)					
	6.0300	3.5300	2.7800	34.6413	22.0000
	6.7000	4.4900	3.0000	60.4803	15.0000
	8.0000	4.6000	3.3300	70.4628	13.0000
	7.8400	4.4900	3.3500	67.5363	25.0000
	7.8400	4.3800	3.3700	64.6514	50.0000
	8.0200	4.3800	3.4200	65.6106	-0.

crust as a P wave. Many of the other apparent arrivals can be identified with particular paths in the layered structure. The largest pulse in all examples shown in Figure 10 corresponds to the direct S wave. In Figure 9 the first arrival in all cases is the direct P wave.

The object of displaying these pulses is not to identify the multiple reflections and converted arrivals but to show the kind of pulse distortion that can be expected from a layered structure and to obtain an estimate of how long a time interval should be considered when doing experimental analysis of real seismograms. In the experimental analysis it will be important to include all the converted waves and

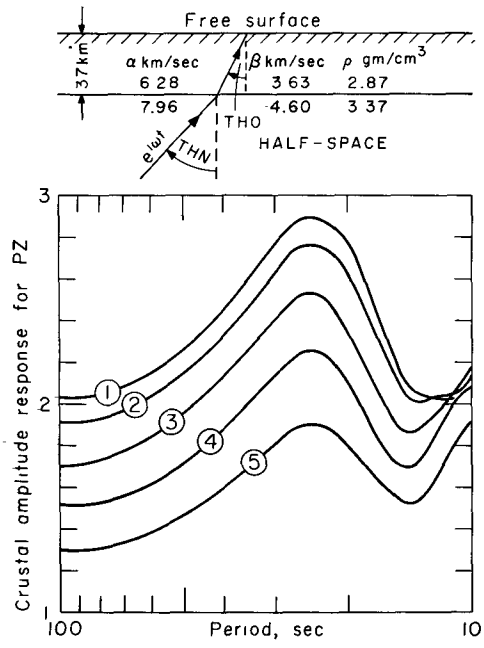

FIG. 1. Variation of crustal amplitude response with the angle of incidence of a dilatational body wave (vertical component) of unit amplitude incident at the bottom of Haskell's unilayered crustal model.

1. C = 48.84 km/sec THN = 10° THO = 7.88°
2. C = 23.27 km/sec THN = 20° THO = 15.66°
3. C = 15.92 km/sec THN = 30° THO = 23.20°
4. C = 12.38 km/sec THN = 40° THO = 30.50°
5. C = 10.39 km/sec THN = 50° THO = 37.20°

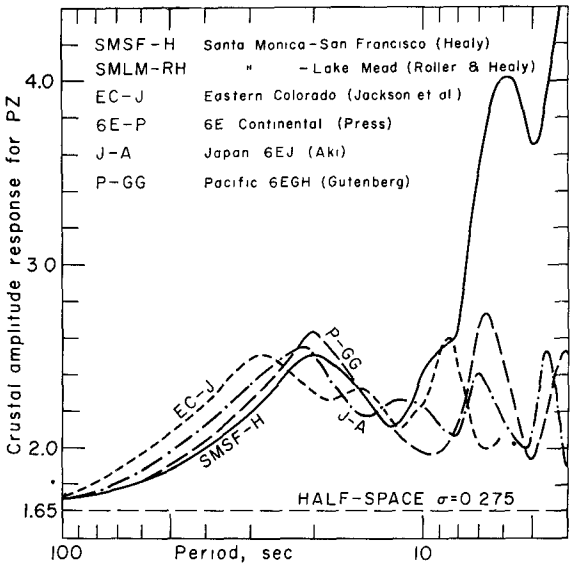

FIG. 2. Role of crustal and subcrustal structure on spectral amplitude response for incident dilatational body wave of unit amplitude and phase velocity of 15 km/sec. (See Table 2 for details of structure.)

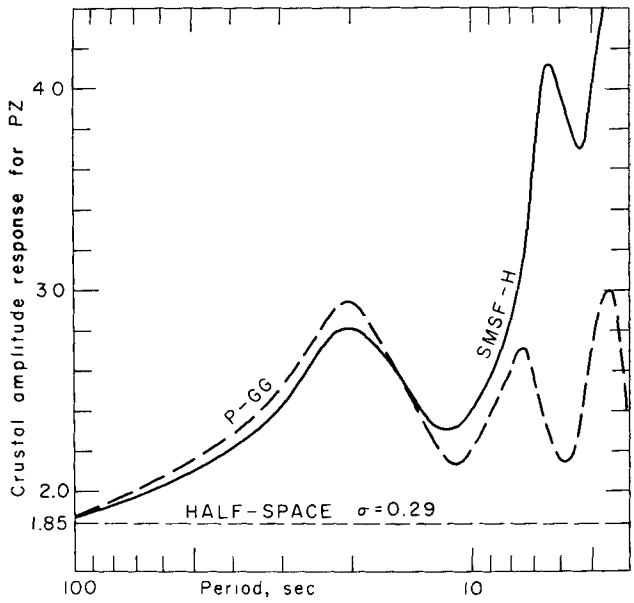

FIG. 3. Spectral amplitude response of an incident dilatational body wave of unit amplitude and phase velocity of 25 km/sec for two different structures.

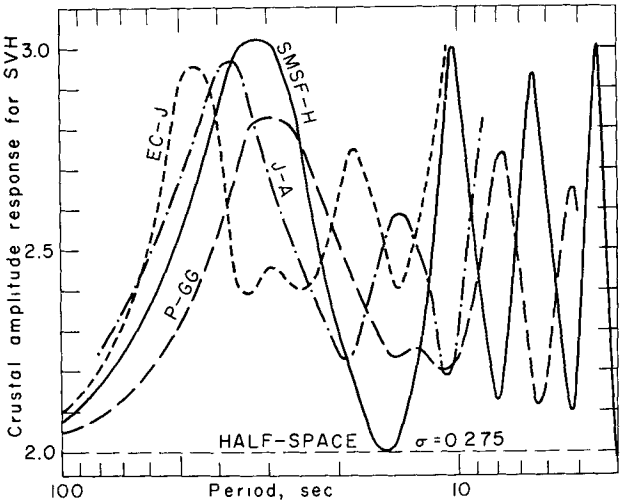

FIG. 4. Crustal and subcrustal spectral amplitude responses to an incident body shear wave (horizontal component of *SV*) of unit amplitude and phase velocity of 25 km/sec.

multiple reverberations in the time sample selected. From Figures 9 and 10 it is clear that a typical time will be 45 seconds. It is important that no other phases interfere during this time interval, so the analysis must be restricted to earthquakes that occur at depths greater than about 300 km where the time for the first reflection from either the free surface or the bottom of the crust is greater than 45 seconds.

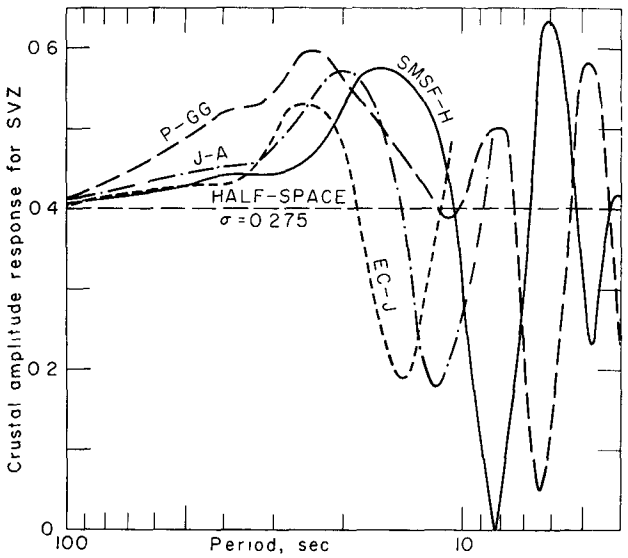

FIG. 5. Crustal and subcrustal amplitude responses to an incident body shear wave (vertical component of SV) of unit amplitude and phase velocity of 25 km/sec.

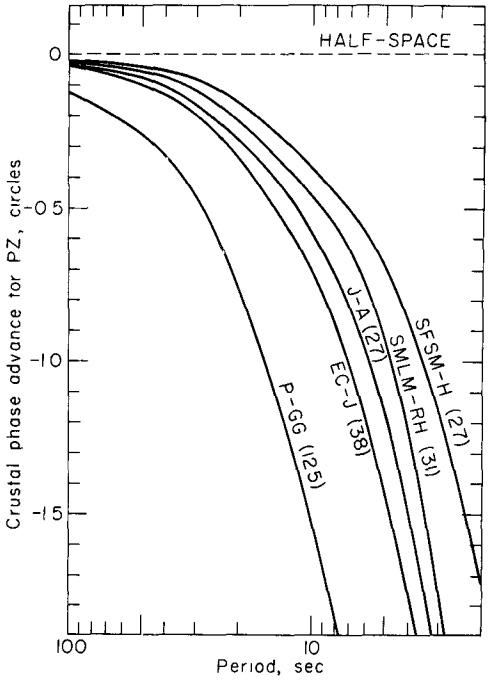

FIG. 6. Phase response of plane dilatational body wave for some crustal models in North America and the Pacific. Numbers indicate depth (in km) at which dilatational plane wave was applied. Wave is incident with phase velocity of 15 km/sec and zero initial phase.

2. *Compensation for Effects of Wave Propagation in the Spherical Earth*

The proper interpretation of the body wave spectrums requires that we establish a correspondence between the particular pulse under consideration and the complete eigenvalue solution in the spherical earth. Ben-Menahem (1964a) used Watson's transformation and the WKBJ approximation to obtain relations between

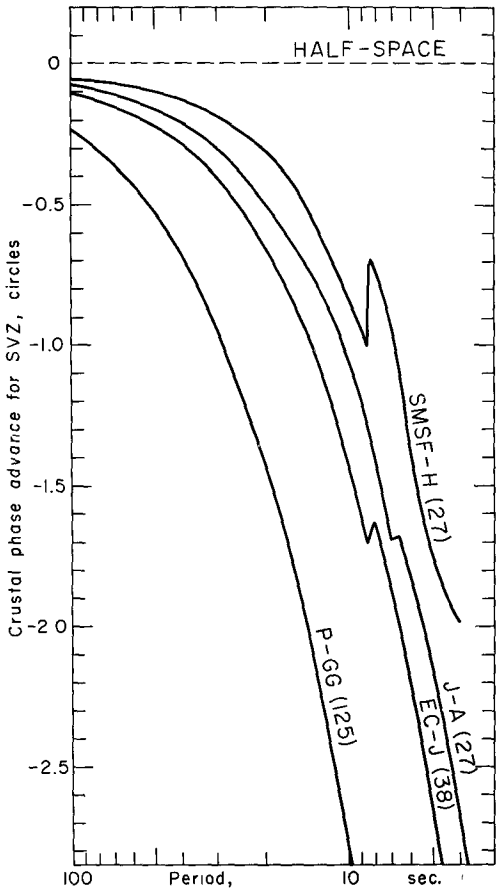

FIG. 7. Phase response of plane shear wave (vertical component) for different structures. Wave is incident with a phase velocity of 25 km/sec and zero initial phase.

the index trio (l, m, n) of a normal mode in a sphere and the corresponding parameters of the ray trajectory associated with this mode. These are given in the form

$$p = a\frac{dt_p}{d\Delta} = \frac{R\sin i}{v(R)} = \frac{l+\frac{1}{2}}{{}_n\omega_l} = \frac{a}{c}$$
$$l < n < \frac{{}_n\omega_l a}{v(a)} \tag{1}$$

where p is the conventional ray parameter, a is the radius of the earth, R is the radial coordinate, l is the order of the normal mode and n is the mode number.

$_n\omega_l$ is the angular frequency of a normal mode, c is the phase velocity of the normal mode (apparent velocity of ray), v is intrinsic body wave velocity of the medium at level R, i is the angle between the radius vector and the tangent to the ray at level R. Finally, $dt_p/d\Delta$ stands for the derivative of the phase travel time t_p with respect to the epicentral distance Δ (km). The spectrum of the direct arrivals of P or S waves at the far field from a dipolar source in a non-absorptive earth, are given approxi-

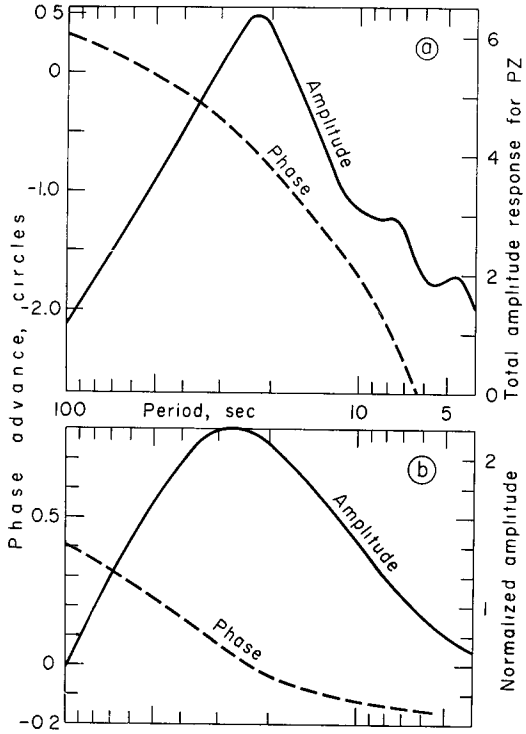

FIG. 8. a. The combined response of a surface layering (P-GG) and a seismograph (30–100 Press-Ewing) to the vertical component of a dilatational body wave of unit amplitude and phase velocity of 25 km/sec. Peak magnification of seismograph is set at 2.2. b. Amplitude and phase response of a 30–100 Press-Ewing long period seismograph system with zero coupling and critical damping.

mately (Bremmer, 1949, Ben-Menahem, 1964a) by

$$U(\omega) = \frac{1}{\sqrt{\sin\vartheta}} \int_{-\infty}^{\infty} f(l;\, {}_n\omega_l)\, \frac{e^{-i\left\{(l+\frac{1}{2})\vartheta + \int_{nr_l}^{a} \sqrt{{}_nk_l^2R^2 - l(l+1)}\,\frac{dR}{R} - \frac{m\pi}{2}\right\}}}{\sqrt{{}_nk_l^2R^2 - l(l+1)}}\, dl \qquad (2)$$

where some numerical constants in front of the integral have been suppressed. The function $f(l;\, {}_n\omega_l)$ represents the amplitude response of the layered earth. It depends on the source-type, the wave-type (P, SH, SV) and on the elastic constants of the layered earth (Gilbert and MacDonald, 1960, Ben-Menahem, 1964b). In equation (2) $\Delta = a\vartheta$, ${}_nk_lv(R) = {}_n\omega_l$ and ${}_nr_l$ is the radius vector to the position $i = \pi/2$. m is the degree of the normal mode. For a non-rotating earth, m will depend only on the source.

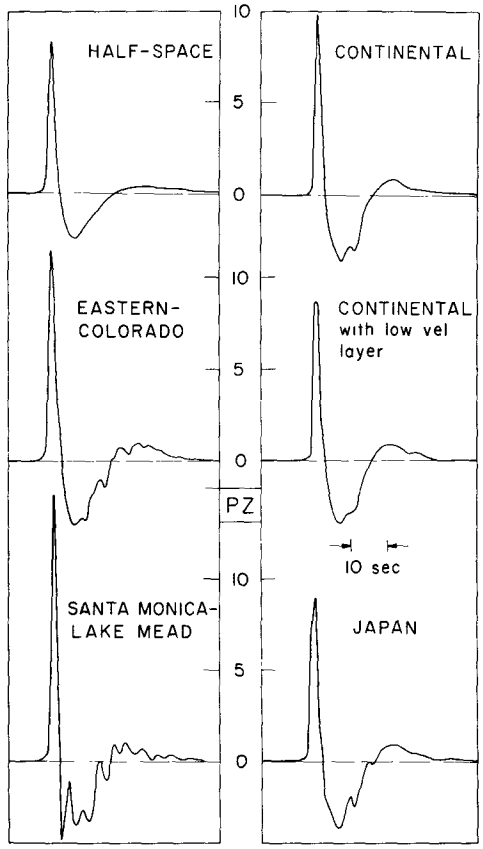

FIG. 9. Synthesized seismograms showing the combined distortion of layering and recording instrument on a plane dilatational body wave pulse with a $\delta(t)$ time function and a phase velocity of 25 km/sec.

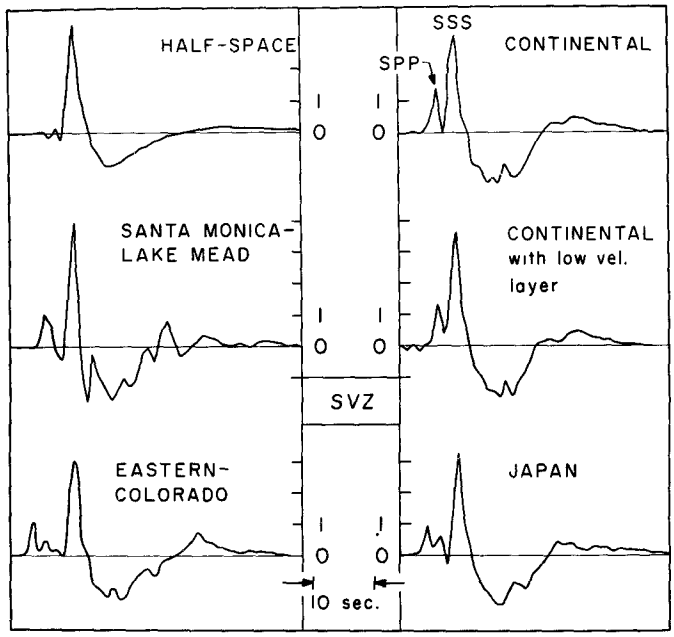

FIG. 10. Synthesized seismograms showing the combined distortion of layering and recording instrument on a plane shear body wave pulse with a $\delta(t)$ time function and a phase velocity of 25 km/sec.

The error term in equation (2) is $O(m^2/l \sin \vartheta)$ with the additional condition $l < n < {}_n\omega_l a/v(a)$, as given in equation (1).

Next, the integral in equation (2) is evaluated by the saddle point method (Bremmer, 1949). It is easy to verify that the saddle point l_0 for the direct arrival is given by

$$\vartheta(l_0) = 2 \int_{nr_l}^{a} \frac{l_0 \, dR}{R\sqrt{{}_nk_l^2R^2 - l_0(l_0 + 1)}} \tag{3}$$

Comparing this expression with its analog in ray theory (Bullen, 1953) we can write the saddle point as $l_0 = {}_n\omega_l \sin i/v(a)$, which in light of equation (2) is Snell's law in disguise. The evaluation of the integral in equation (2) at the saddle point $l = l_0$ contributes the factor $1/a \mid d^2\chi(l_0)/dl_0^2 \mid^{-1/2} l_0^{1/2} (\cos i)^{-1}$, where $\chi(l_0)$ is the phase of the integrand. But since $\mid d^2\chi(l_0)/dl_0^2 \mid = \mid d\vartheta(l_0)/dl_0 \mid$ we obtain the well known divergence factor D,

$$D = \frac{1}{a}\sqrt{\left|\frac{\tan i_0}{\sin \vartheta}\frac{di_0}{d\vartheta}\right|} \tag{4}$$

For a deep source we must replace $di_0/d\vartheta \tan i_0$ by $(\sin i_h/\cos i_0)(di_h/d\vartheta)$ where i_h is the angle of emergence of the ray at the source and i_0 is the angle of incidence of the ray at the base of the low velocity layer. The case $di_h/d\vartheta = 0$ indicates the presence of a caustic and requires a third order saddle point approximation.

The divergence factor can be obtained by simple geometric arguments (Jeffreys, 1926) or equivalently from the Eikonal function with the aid of Gauss's theorem (Karal and Keller, 1959).

The initial phase $\phi_0(\omega)$ of the direct P and S waves is obtained from the spectrums of these waves analogous to its derivation from the spectrums of surface waves. Namely,

$$\phi_0(\omega) = f\left(\frac{\Delta}{c} - t_0\right) + \text{Fourier phase} + [n(\omega) - 1] - \varphi_{\text{inst.}} - (\delta\varphi)_{\text{crust}} . \tag{5}$$

In this expression c is the phase velocity, assumed to be common to all the modes which constitute the isolated signal. t_0 is the difference between the time of origin and the first arrival of the pulse. The Fourier phase is also measured relative to this fiducial time. The mode number function $n(\omega)$ for the propagating body wave is that introduced and measured by Brune (1964b). The function $(\delta\varphi)_{\text{crust}}$ is the excessive phase advance due to the crust below the recording station. It is assumed that the mantle does not introduce phase shift other than those which are already included in the term $f(t - \Delta/c)$.

It remains to compensate for the loss of energy due to the anelasticity of the mantle. Recent studies in this field (Anderson and Archambeau, 1964) express the departure from pure elasticity by the intrinsic Q function which depends on the depth alone. Thus the total attenuation of a given angular frequency ω along a given ray is governed by the factor $\exp\{-\int \gamma(\omega, s)\, ds\}$ where s is the ray parameter

and $\gamma(\omega, s)$ is the attenuation coefficient along the ray. Inserting

$$ds = \frac{\eta\, dR}{\sqrt{\eta^2 - p^2}}; \qquad \gamma(\omega, s) = \frac{\omega}{2Q(R)v(R)}; \qquad \eta = \frac{R}{v(R)} \tag{6}$$

Making use of equation (1), we obtain the total attenuation *correction*

$$\log \text{ (attenuation correction)} = \frac{\omega}{2}\int_{\text{ray}} \frac{\eta^2}{\sqrt{\eta^2 - p^2}} \frac{dR}{RQ(R)} = \omega g(\Delta; h) \tag{7}$$

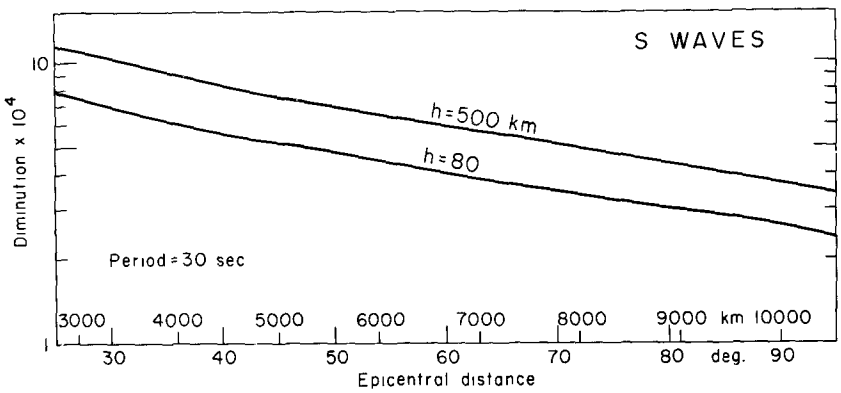

FIG. 11. Total diminution of a spectral component of a *S*-wave due to divergence and attenuation along its ray for a realistic spherical earth model.

The integration is performed along the radius from the source level to the bottom of the ray and from there to the free surface, including the crust.

It is assumed that Q is independent of frequency. Causal phase shifts are neglected. For a constant $Q = Q_0$, the attenuation is approximately given by $\exp\{-\omega\tau/2Q_0\}$, τ being the travel time along the ray, as given in the Jeffreys-Bullen tables.

The total diminution $De^{-\omega g(\Delta;h)}$ which combines the effects of divergence and attenuation is shown in Figure 11, for the spectral period $T = 30$ sec. It was computed for this period and others with the aid of $(i - \Delta)$ curves of Ritsema (1958). Attenuation correction was obtained by numerical integration for a Bullen *A* velocity-depth profile (Bullen, 1953) and model *H* for $Q(R)$ (Anderson and Archambeau, 1964). The numerical evaluation of the function $g(\Delta, h)$ led to the approximation:

$$g(\Delta; h) \approx \frac{a}{v(a)} \left| \frac{\sin(i_h - i_0)}{\sin i_h} \right| 10^{-3} \text{ sec} \tag{8}$$

where i_h is measured from the vertical to the tangent of the ray ($0 \leqq i_h \leqq 360°$, $0 \leqq i_0 \leqq 90°$) as shown in Figure 12. A typeout of a routine program which computes the attenuation and the divergence coefficients for a set of rays emanating

from a given depth, is shown in Table 3. The columns from left to right read: epicentral distance in degrees, epicentral distance in km, angle of emergence in degrees, angle of incidence in degrees, divergence factor D, the attenuation factor $\exp\{-\omega g(\Delta, h)\}$, the total diminution and its reciprocal. Note the slow variation of the attenuation with both the epicentral distance and the sources depth, for $\Delta > 24°$.

3. *Point-Source Models and Their Radiation Patterns*

For the purpose of our study it is sufficient to assume that the source is imbedded in a homogeneous bulk of elastic material which extends over a region that is small

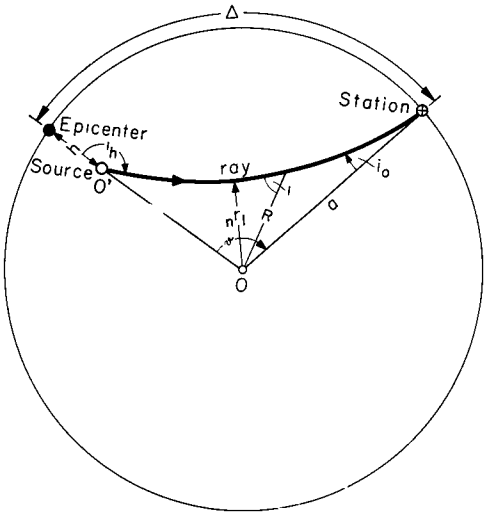

FIG. 12. Curved ray path in the earth and ray parameters.

as compared to the epicentral distance of the nearest station. Let k_α, k_β be the longitudinal and shear wave numbers respectively in the source's linear region. The spectral displacement field on the boundary of this region is assumed to be solutions of the Helmholtz vector wave equation,

$$\mathbf{U} = -\frac{1}{k_\alpha^2}\,\text{grad div}\,\mathbf{U} + \frac{1}{k_\beta^2}\,\text{curl curl}\,\mathbf{U} \tag{9}$$

with a given distribution function for the initial displacement vector U_0 at the source.

The general solution of this equation, written in the compact operational notation of Morse and Feshbach (1953, Chap. 13)

$$4\pi\mathbf{U}_P = v_p^2 \oint \{(G_p\cdot\mathbf{n})\,\text{div}\,\mathbf{U}_0 - (\mathbf{U}_0\cdot\mathbf{n})\,\text{div}\,G_p\}\,dS \tag{10}$$

TABLE 3

COMBINED ATTENUATION AND DIVERGENCE FACTORS FOR T = 30 SEC.

DI/DDELTA -0.44 DEPTH 376.00KM VO 7.70KM/SEC VH 8.86KM/SEC RHOO 3.32 RHOH 3.61

DIST(DEG)	DIST(KM)	IH	IO	DIV	ATT	DIMINU	1/DIMINU
24.00	2666.64	128.56	42.55	0.001255	0.916	0.0011492	870.18
25.00	2777.75	129.00	42.23	0.001222	0.915	0.0011189	893.71
26.00	2888.86	129.44	41.91	0.001192	0.915	0.0010903	917.17
27.00	2999.97	129.88	41.58	0.001163	0.914	0.0010632	940.58
28.00	3111.08	130.32	41.25	0.001135	0.914	0.0010374	963.95
29.00	3222.19	130.76	40.93	0.001109	0.913	0.0010129	987.30
30.00	3333.30	131.20	40.60	0.001084	0.913	0.0009895	1010.64
31.00	3444.41	131.64	40.27	0.001060	0.912	0.0009671	1033.99
32.00	3555.52	132.08	39.93	0.001038	0.912	0.0009457	1057.36
33.00	3666.63	132.52	39.60	0.001016	0.911	0.0009253	1080.76
34.00	3777.74	132.96	39.27	0.000995	0.910	0.0009056	1104.21
35.00	3888.85	133.40	38.93	0.000975	0.910	0.0008867	1127.72
36.00	3999.96	133.84	38.59	0.000955	0.909	0.0008686	1151.29
37.00	4111.07	134.28	38.26	0.000936	0.909	0.0008511	1174.94
38.00	4222.18	134.72	37.92	0.000918	0.908	0.0008342	1198.67
39.00	4333.29	135.16	37.58	0.000901	0.908	0.0008180	1222.51
40.00	4444.40	135.60	37.24	0.000884	0.907	0.0008023	1246.45
41.00	4555.51	136.04	36.89	0.000868	0.907	0.0007871	1270.51
42.00	4666.62	136.48	36.55	0.000852	0.906	0.0007724	1294.69
43.00	4777.73	136.92	36.21	0.000837	0.906	0.0007581	1319.01
44.00	4888.84	137.36	35.86	0.000822	0.905	0.0007443	1343.47
45.00	4999.95	137.80	35.52	0.000808	0.905	0.0007309	1368.09
46.00	5111.06	138.24	35.17	0.000794	0.904	0.0007179	1392.86
47.00	5222.17	138.68	34.82	0.000780	0.904	0.0007053	1417.81
48.00	5333.28	139.12	34.47	0.000767	0.903	0.0006930	1442.94
49.00	5444.39	139.56	34.12	0.000754	0.903	0.0006811	1468.26
50.00	5555.50	140.00	33.77	0.000742	0.902	0.0006694	1493.77
51.00	5666.61	140.44	33.42	0.000730	0.902	0.0006581	1519.50
52.00	5777.72	140.88	33.07	0.000718	0.901	0.0006471	1545.43
53.00	5888.83	141.32	32.72	0.000706	0.901	0.0006363	1571.60
54.00	5999.94	141.76	32.36	0.000695	0.900	0.0006258	1598.00
55.00	6111.05	142.20	32.01	0.000684	0.900	0.0006155	1624.65
56.00	6222.16	142.64	31.66	0.000673	0.900	0.0006055	1651.56
57.00	6333.27	143.08	31.30	0.000663	0.899	0.0005957	1678.73
58.00	6444.38	143.52	30.94	0.000652	0.899	0.0005861	1706.17
59.00	6555.49	143.96	30.59	0.000642	0.898	0.0005767	1733.91
60.00	6666.60	144.40	30.23	0.000632	0.898	0.0005675	1761.95
61.00	6777.71	144.84	29.87	0.000622	0.897	0.0005586	1790.29
62.00	6888.82	145.28	29.51	0.000613	0.897	0.0005498	1818.96
63.00	6999.93	145.72	29.15	0.000604	0.897	0.0005411	1847.97
64.00	7111.04	146.16	28.79	0.000594	0.896	0.0005327	1877.32
65.00	7222.15	146.60	28.43	0.000585	0.896	0.0005244	1907.04
66.00	7333.26	147.04	28.07	0.000577	0.895	0.0005162	1937.13
67.00	7444.37	147.48	27.71	0.000568	0.895	0.0005082	1967.61
68.00	7555.48	147.92	27.34	0.000559	0.894	0.0005004	1998.49
69.00	7666.59	148.36	26.98	0.000551	0.894	0.0004927	2029.80
70.00	7777.70	148.80	26.62	0.000543	0.894	0.0004851	2061.54
71.00	7888.81	149.24	26.25	0.000535	0.893	0.0004776	2093.74
72.00	7999.92	149.68	25.89	0.000527	0.893	0.0004703	2126.41
73.00	8111.03	150.12	25.52	0.000519	0.893	0.0004631	2159.57
74.00	8222.14	150.56	25.16	0.000511	0.892	0.0004559	2193.24
75.00	8333.25	151.00	24.79	0.000503	0.892	0.0004489	2227.44
76.00	8444.36	151.44	24.42	0.000496	0.891	0.0004420	2262.19
77.00	8555.47	151.88	24.06	0.000488	0.891	0.0004352	2297.52
78.00	8666.58	152.32	23.69	0.000481	0.891	0.0004285	2333.44
79.00	8777.69	152.76	23.32	0.000474	0.890	0.0004219	2369.99
80.00	8888.80	153.20	22.95	0.000467	0.890	0.0004154	2407.19
81.00	8999.91	153.64	22.58	0.000460	0.890	0.0004090	2445.06
82.00	9111.02	154.08	22.21	0.000453	0.889	0.0004026	2483.65
83.00	9222.13	154.52	21.84	0.000446	0.889	0.0003964	2522.97
84.00	9333.24	154.96	21.47	0.000439	0.889	0.0003902	2563.07
85.00	9444.35	155.40	21.10	0.000432	0.888	0.0003840	2603.97
86.00	9555.46	155.84	20.73	0.000426	0.888	0.0003780	2645.71
87.00	9666.57	156.28	20.36	0.000419	0.888	0.0003720	2688.34
88.00	9777.68	156.72	19.99	0.000412	0.888	0.0003660	2731.90
89.00	9888.79	157.16	19.62	0.000406	0.887	0.0003602	2776.43
90.00	9999.90	157.60	19.24	0.000400	0.887	0.0003544	2821.97
91.00	10111.01	158.04	18.87	0.000393	0.887	0.0003486	2868.59
92.00	10222.12	158.48	18.50	0.000387	0.886	0.0003429	2916.33
93.00	10333.23	158.92	18.12	0.000381	0.886	0.0003372	2965.26
94.00	10444.34	159.36	17.75	0.000374	0.886	0.0003316	3015.44
95.00	10555.45	159.80	17.38	0.000368	0.886	0.0003261	3066.93
96.00	10666.56	160.24	17.00	0.000362	0.885	0.0003205	3119.81
97.00	10777.67	160.68	16.63	0.000356	0.885	0.0003150	3174.16
98.00	10888.78	161.12	16.25	0.000350	0.885	0.0003096	3230.06
99.00	10999.89	161.56	15.88	0.000344	0.885	0.0003042	3287.60

$$4\pi \mathbf{U}_S = -v_s^2 \oint \{[G_s \cdot (\mathbf{n} \times \text{curl } \mathbf{U}_0)] + [\text{curl } G_s \cdot (\mathbf{n} \times \mathbf{U}_0)]\}\, dS \qquad (11)$$

Here $\mathbf{U}_P$ and $\mathbf{U}_S$ are the longitudinal and shear vectorial displacement fields on the boundary of the source region, n is the outer normal to a surface S surrounding the source, G_P and G_S are the corresponding Green dyadics for the compressional and shear waves.

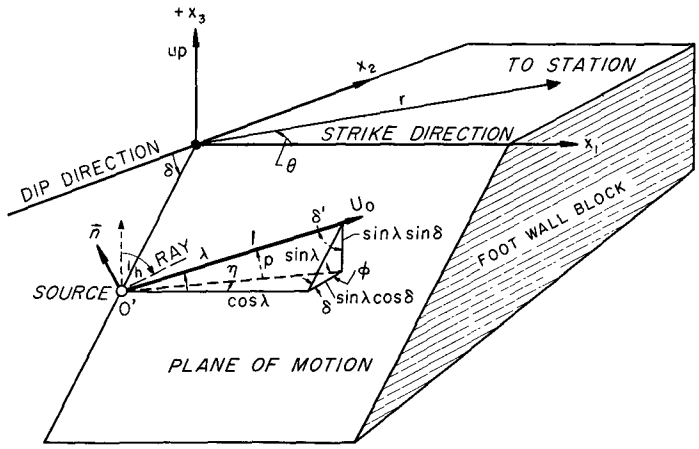

FIG. 13. Geometry of source elements and relative position of station on the free surface.

$$G_P = \frac{1}{v_p^2} \frac{e^{-ik_\alpha R}}{R} \mathbf{RR}$$
$$G_S = \frac{1}{v_s^2} \frac{e^{-ik_\beta R}}{R} (\boldsymbol{\theta\theta} + \boldsymbol{\varphi\varphi}) \qquad (12)$$

The displacement vector $\mathbf{U}_0$ is chosen as a spatial delta function of strength L_0, step function in time and directed along a unit vector $\mathbf{a}$

$$\mathbf{U}_0 = \mathbf{U}_+ - \mathbf{U}_- = L_0 \left\{ \frac{e^{i\omega t}}{i\omega} \right\} \delta(R - R_0)\mathbf{a} \qquad (13)$$

We next set up two coordinate systems at the source: a spherical system (R, θ, i_h) with a right hand base $(\mathbf{R\theta\varphi})$ and a cartesian system $(x_1x_2x_3)$ with a right hand base $(e_1e_2e_3)$, as shown in Figure 13. Two types of displacement faults will be considered; shear faults in which the displacement vector is in the fault plane and tensile faults for which the displacements are perpendicular to the fault. The first is equivalent to a double couple force system while the second is equivalent to a force dipole (without a moment) normal to the fault with a superimposed purely compressional component (Knopoff and Gilbert, 1960, Haskell, 1964). Considering point sources of

these types we may assume that the integrands in equation (10) remain constant over the infinitesimal source area which consists of the two sides of a plane of area dS with a normal $\mathbf{n}$.

We next evaluate the integrands of equations (10) and (11) according to the laws of the calculus of dyadics (Morse and Feshbach, 1953, chap. 1).

$$\operatorname{div} G_P = \frac{-ik_\alpha}{v_p^2}\left\{\frac{e^{-ik_\alpha R}}{R}\right\}\mathbf{R} + O\left(\frac{1}{R^2}\right) \tag{14}$$

$$\operatorname{curl} G_S = \frac{-ik_\beta}{v_s^2}\left\{\frac{e^{-ik_\beta R}}{R}\right\}(\varphi\boldsymbol{\theta} - \boldsymbol{\theta}\varphi) + O\left(\frac{1}{R^2}\right) \tag{15}$$

$$\operatorname{div} \mathbf{U}_0 = -L_0\left\{\frac{e^{i\omega t}}{i\omega}\right\}\delta'(R - R_0)(\mathbf{a}\cdot\mathbf{R}) \tag{16}$$

$$\operatorname{curl} \mathbf{U}_0 = L_0\left\{\frac{e^{i\omega t}}{i\omega}\right\}\delta'(R - R_0)[(\mathbf{a}\cdot\boldsymbol{\theta})\varphi - (\mathbf{a}\cdot\varphi)\boldsymbol{\theta}] \tag{17}$$

Inserting these expressions into the integrands and integrating over an infinitesimal surface, we finally obtain for a shear fault with a step-function time dependence.

$$\begin{aligned}
\mathbf{U}_P &= \left\{\frac{L_0\, dS}{2\pi v_p}\left(\frac{v_s}{v_p}\right)^2\right\}(\mathbf{a}\cdot\mathbf{R})(\mathbf{n}\cdot\mathbf{R})\mathbf{R} \\
\mathbf{U}_{SV} &= \left\{\frac{L_0\, dS}{4\pi v_s}\right\}[(\mathbf{n}\cdot\mathbf{R})(\mathbf{a}\cdot\varphi) + (\mathbf{a}\cdot\mathbf{R})(\mathbf{n}\cdot\varphi)]\varphi \\
\mathbf{U}_{SH} &= \left\{\frac{L_0\, dS}{4\pi v_s}\right\}[(\mathbf{n}\cdot\mathbf{R})(\mathbf{a}\cdot\boldsymbol{\theta}) + (\mathbf{a}\cdot\mathbf{R})(\mathbf{n}\cdot\boldsymbol{\theta})]\boldsymbol{\theta}
\end{aligned} \tag{18}$$

For a tensile fault with the same time function and

$$\mathbf{U}_0 = L_0\left\{\frac{e^{i\omega t}}{i\omega}\right\}\delta(R - R_0)\mathbf{n}$$

we find

$$\begin{aligned}
\mathbf{U}_P &= \left\{\frac{L_0\, dS}{2\pi v_p}\left(\frac{v_s}{v_p}\right)^2\right\}[s_0 + (\mathbf{n}\cdot\mathbf{R})^2]\mathbf{R} \qquad s_0 = \frac{\sigma(h)}{1 - 2\sigma(h)} \\
\mathbf{U}_{SV} &= \left\{\frac{L_0\, dS}{2\pi v_s}\right\}(\mathbf{n}\cdot\mathbf{R})(\mathbf{n}\cdot\varphi)\varphi \\
\mathbf{U}_{SH} &= \left\{\frac{L_0\, dS}{2\pi v_s}\right\}(\mathbf{n}\cdot\mathbf{R})(\mathbf{n}\cdot\boldsymbol{\theta})\boldsymbol{\theta}
\end{aligned} \tag{19}$$

where the factors $\exp\,[i\omega(t - R/v_p)]/R$ and $\exp\,[i\omega(t - R/v_s)]/R$ were suppressed and terms of the order $(1/R)^2$ were deleted. $\sigma(h)$ is the poisson ratio at depth.

To obtain the radiation field we first express all unit vectors in terms of the base $(\mathbf{e}_1\mathbf{e}_2\mathbf{e}_3)$.

$$\begin{aligned}
\mathbf{a} &= \cos\lambda\mathbf{e}_1 + \sin\lambda\cos\delta\mathbf{e}_2 + \sin\lambda\sin\delta\mathbf{e}_3 \\
\mathbf{n} &= -\sin\delta\mathbf{e}_2 + \cos\delta\mathbf{e}_3 \\
\mathbf{R} &= \sin i_h\cos\theta\mathbf{e}_1 + \sin i_h\sin\theta\mathbf{e}_2 + \cos i_h\mathbf{e}_3 \\
\boldsymbol{\theta} &= -\sin\theta\mathbf{e}_1 + \cos\theta\mathbf{e}_2 \\
\boldsymbol{\varphi} &= \cos i_h\cos\theta\mathbf{e}_1 + \cos i_h\sin\theta\mathbf{e}_2 - \sin i_h\mathbf{e}_3
\end{aligned} \tag{20}$$

TABLE 4

VERTICAL RADIATION PATTERNS FOR THE FAR FIELD OF BODY WAVES

$A(i_h) = \mathbf{c}_0 + \mathbf{c}_1\sin i_h + d_1\cos i_h + \mathbf{c}_2\sin 2i_h + d_2\cos 2i_h$

$\Omega_1 = \cos\theta\cos\lambda + \sin\theta\sin\lambda\cos\delta$

$\Omega_2 = \cos\theta\cos\lambda\cos\delta + \sin\theta\sin\lambda\cos 2\delta$

$\Omega_3 = \sin 2\theta\sin\lambda\cos\delta + \cos 2\theta\cos\lambda$

$\Omega_4 = \cos\theta\cos 2\delta\sin\lambda - \sin\theta\cos\lambda\cos\delta$

		c_o	c_1	d_1	c_2	d_2
P	shear fault	$\frac{1}{4}\sin\lambda\sin 2\delta - \frac{1}{2}\sin\theta\sin\delta\,\Omega_1$	0	0	$\frac{1}{2}\Omega_2$	$\frac{1}{4}\sin\lambda\sin 2\delta + \frac{1}{2}\sin\theta\sin\delta\,\Omega_1$
	tensile fault	$s_0 + \frac{1}{2} - \frac{1}{4}\sin^2\delta(1+\cos 2\theta)$	0	0	$-\frac{1}{2}\sin 2\delta\sin\theta$	$\frac{1}{4}[2+\sin^2\delta(\cos 2\theta - 3)]$
SH	shear fault	0	$-\sin\delta\,\Omega_3$	Ω_4	0	0
	tensile fault	0	$-\frac{1}{2}\sin^2\delta\sin 2\theta$	$\frac{1}{2}\sin 2\delta\cos\theta$	0	0
SV	shear fault	0	0	0	$-\frac{1}{2}\sin\lambda\sin 2\delta - \sin\theta\sin\delta\,\Omega_1$	Ω_2
	tensile fault	0	0	0	$\frac{1}{4}[(1-3\cos^2\delta) - \sin^2\delta\cos 2\theta]$	$-\frac{1}{2}\sin\theta\sin 2\delta$

The explicit expressions for the radiation patterns from faults of arbitrary dip and slip are obtained in a straight forward fashion by the combined use of equations (18), (19) and (20). The final results were assembled in Tables 4 and 5. Some typical cases have been calculated and these are presented in Figures 14–18. All patterns obey the symmetry relations:

$$\text{Amp}\ (\theta; i_h) = \text{Amp}\ (\theta; i_h \pm 180°)\ P \text{ and } SV \tag{21}$$

$$\text{Amp}\ (\theta; i_h) = -\text{Amp}\ (\theta; i_h \pm 180°)\ SH \tag{22}$$

$$\text{Amp}\ (\theta; i_h) = \pm\ \text{Amp}\ (\theta + 180°; 360° - i_h) \tag{23}$$

where the plus sign is for P waves and the minus sign for S waves.

$$\text{Amp}\ (\lambda + 180°) = -\ \text{Amp}\ (\lambda) \quad \text{for shear faults} \tag{24}$$

$$\text{Amp}\ (\theta; \delta) = \text{Amp}\ (\theta + 180°; 180 - \delta) \quad \text{for tensile faults} \tag{25}$$

Unlike the surface wave patterns there is no azimuthal symmetry and in general Amp (θ) is not equal to Amp $(\theta + 180°)$. All patterns are three-dimensional. It

TABLE 5

HORIZONTAL RADIATION PATTERNS FOR THE FAR FIELD OF BODY WAVES

$A(\theta) = a_0 + a_1 \sin\theta + b_1 \cos\theta + a_2 \sin 2\theta + b_2 \cos 2\theta \qquad Q_0 = \frac{1}{4}(4s_0 + 2 - \sin^2\delta)$

		a_0	a_1	b_1	a_2	b_2
P	shear fault	$\frac{1}{4}\sin\lambda\sin 2\delta\cdot(3\cos^2 i_h - 1)$	$\frac{1}{2}\sin\lambda\cos 2\delta\sin 2i_h$	$\frac{1}{2}\cos\lambda\cos\delta\sin 2i_h$	$-\frac{1}{2}\cos\lambda\sin\delta\sin^2 i_h$	$\frac{1}{4}\sin\lambda\sin 2\delta\sin^2 i_h$
	tensile fault	$Q_0 + \frac{1}{4}(2 - 3\sin^2\delta)\cdot\cos 2i_h$	$-\frac{1}{2}\sin 2\delta\sin 2i_h$	0	0	$\frac{1}{4}\sin^2\delta(\cos 2\iota - 1)$
SH	shear fault	0	$-\cos\lambda\cos\delta\cos i_h$	$\sin\lambda\cos 2\delta\cos\iota_h$	$-\frac{1}{2}\sin\lambda\sin 2\delta\sin i_h$	$-\cos\lambda\sin\delta\sin i_h$
	tensile fault	0	0	$-\frac{1}{2}\sin 2\delta\cos i_h$	$\frac{1}{2}\sin^2\delta\sin i_h$	0
SV	shear fault	$-\frac{3}{4}\sin\lambda\sin 2\delta\cdot\sin 2\iota_h$	$\sin\lambda\cos 2i_h\cos 2\delta$	$\cos\lambda\cos\delta\cos 2\iota_h$	$-\frac{1}{2}\cos\lambda\sin\delta\sin 2\iota_h$	$\frac{1}{4}\sin\lambda\sin 2\delta\sin 2\iota_h$
	tensile fault	$\frac{1}{4}\sin 2i_h\cdot(1 - 3\cos^2\delta)$	$-\frac{1}{2}\cos 2i_h\sin 2\delta$	0	0	$-\frac{1}{4}\sin 2\iota_h\sin^2\delta$

can be visualized by observing simultaneously the azimuthal and vertical cross sections as shown in Figures 14–18. Radiation patterns for shear and tensile faults with arbitrary parameters can easily be computed with the aid of the simple trigonometric coefficients given in Tables 4 and 5. Samples of computer outputs are shown in Tables 6–9. It includes the calculation of the polarization angle, defined as the phase of a complex number,

$$\epsilon = \text{phase}\ [U_{SV} + iU_{SH}] \tag{26}$$

where U_{SV} and U_{SH} are given in equations (18) and (19). This angle is given in units of degrees and circles for both azimuthal and vertical patterns. Figure 19 shows the variation of ϵ with the fault elements. The polarization angle can be ex-

pressed analytically for the case of shear faults in the form,

$$\tan \epsilon = \frac{\cos i_h \sin (\theta - \gamma) |\cos q| + \sin i_h |\cos p| \sin \delta \cos (2\theta - \eta)}{\frac{1}{2} \sin 2i_h |\cos p| \sin \delta [3 \sin \eta + \sin (2\theta - \eta)] - \cos 2i_h |\cos q| \cos (\theta - \gamma)} \quad (27)$$

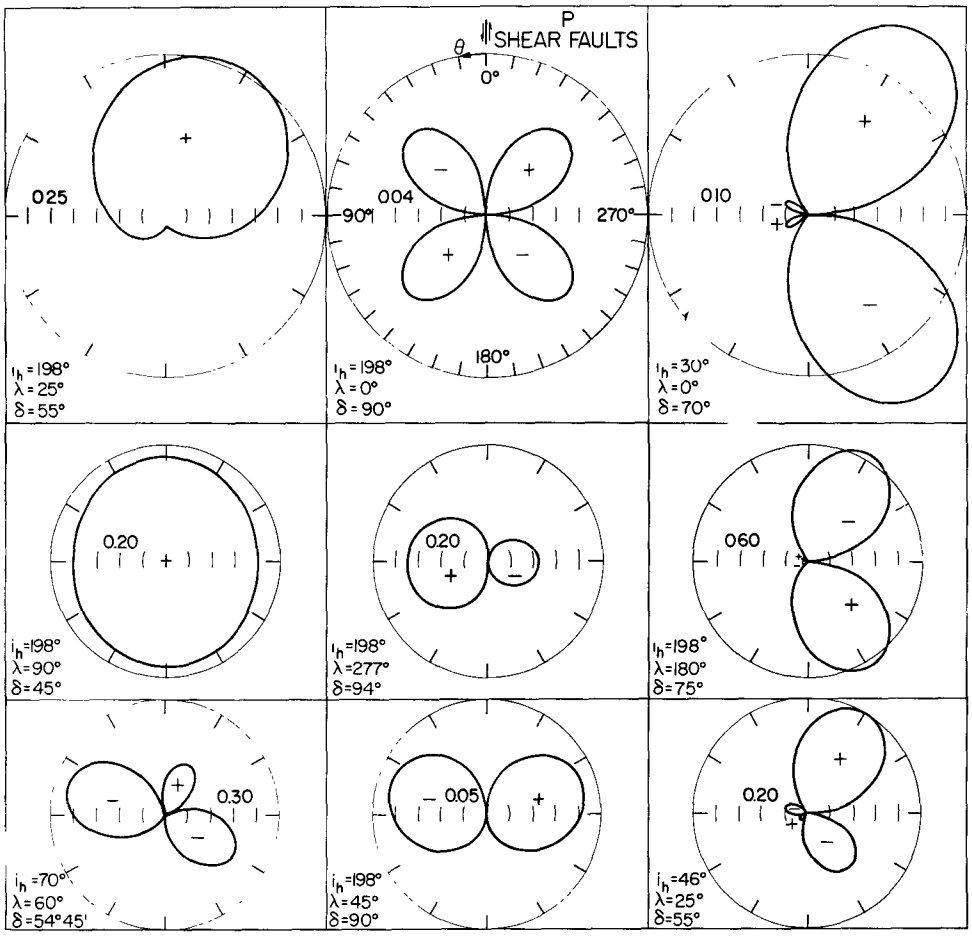

FIG. 14. Horizontal radiation patterns of the far field of P waves in a boundless elastic medium from shear type point sources. Positive and negative signs indicates compression (outward motion in source coordinates) and dilatation respectively.

and as

$$\tan \epsilon = \frac{\cos \theta \tan \delta}{\cos i_h \sin \theta \tan \delta + \sin i_h} \quad (28)$$

for tensile faults. p is the plunge angle, η is the azimuth of the trend and q and γ are defined in terms of the dip angle and the slip angle by

$$\cos\delta\cos\lambda = \cos\gamma\,|\cos q\,|$$

$$\cos\gamma = \frac{\cos\lambda\cos\delta}{\sqrt{\cos^2\lambda\cos^2\delta + \sin^2\lambda\cos^2 2\delta}} \tag{29}$$

The same angles appear in the expressions for the radiation patterns of surface waves (Ben-Menahem and Harkrider, 1964).

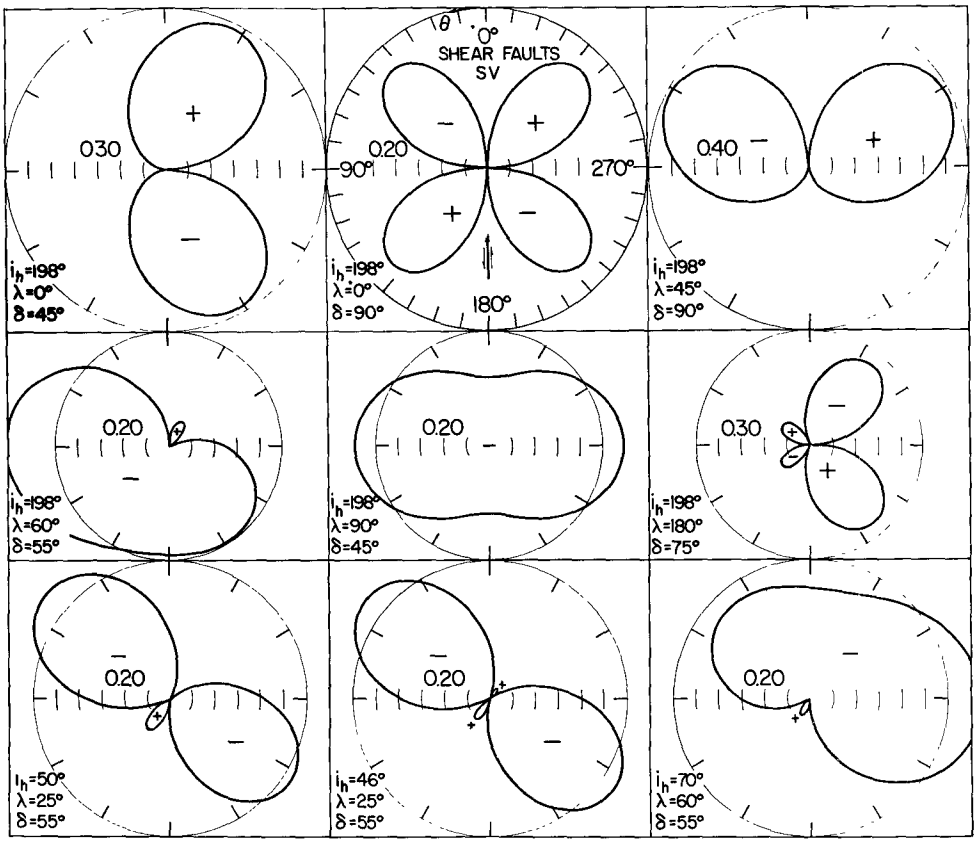

FIG. 15. Horizontal radiation patterns of the far field of *SV* waves in a boundless elastic medium from shear type point sources. Positive sign refers to clockwise motion in the vertical plane θ = const in source coordinates (*SVH* on downgoing rays changes sign in the real earth).

4. *A Test for a Propagating Source*

A departure from a localized source may result in frequency-dependent patterns and initial phases which are azimuth-dependent. Both effects are observable only if the dimensions of the source are of the order of the observable wavelengths. Data processing of surface wave spectrums of major shallow earthquakes revealed that a uniformly propagating rupture took place along a finite fault (Ben-Menahem and Toksoz, 1963). To test this hypothesis against the spectrums of body waves we

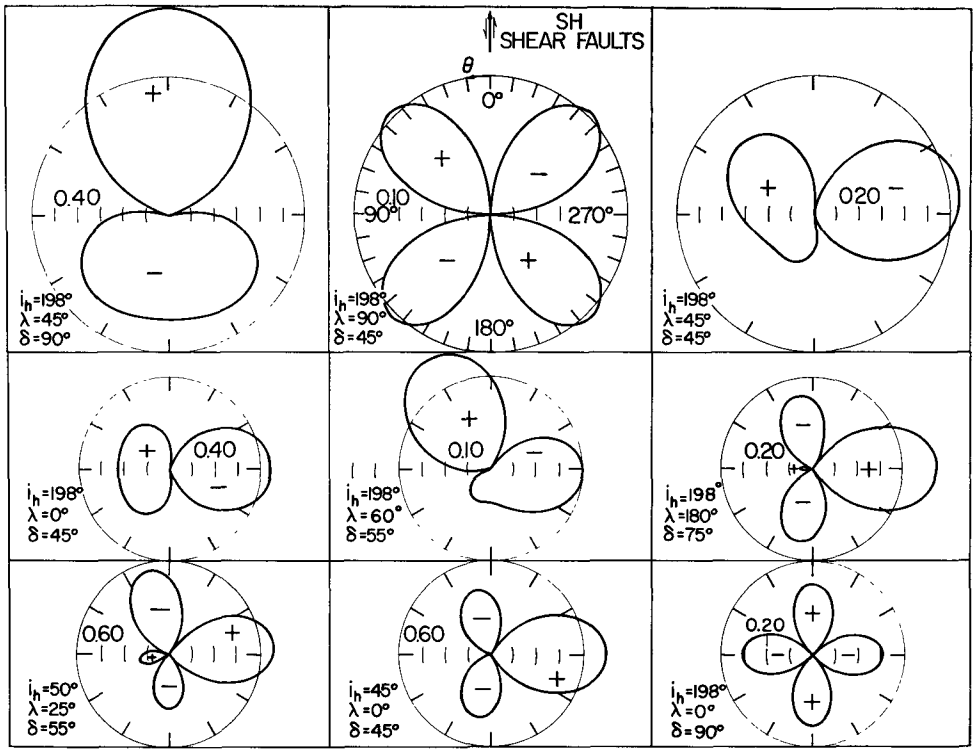

FIG. 16. Horizontal radiation patterns of the far field of *SH* waves in a boundless elastic medium from shear type point sources. Positive sign indicates counterclockwise motion in the cone φ = const in source coordinates.

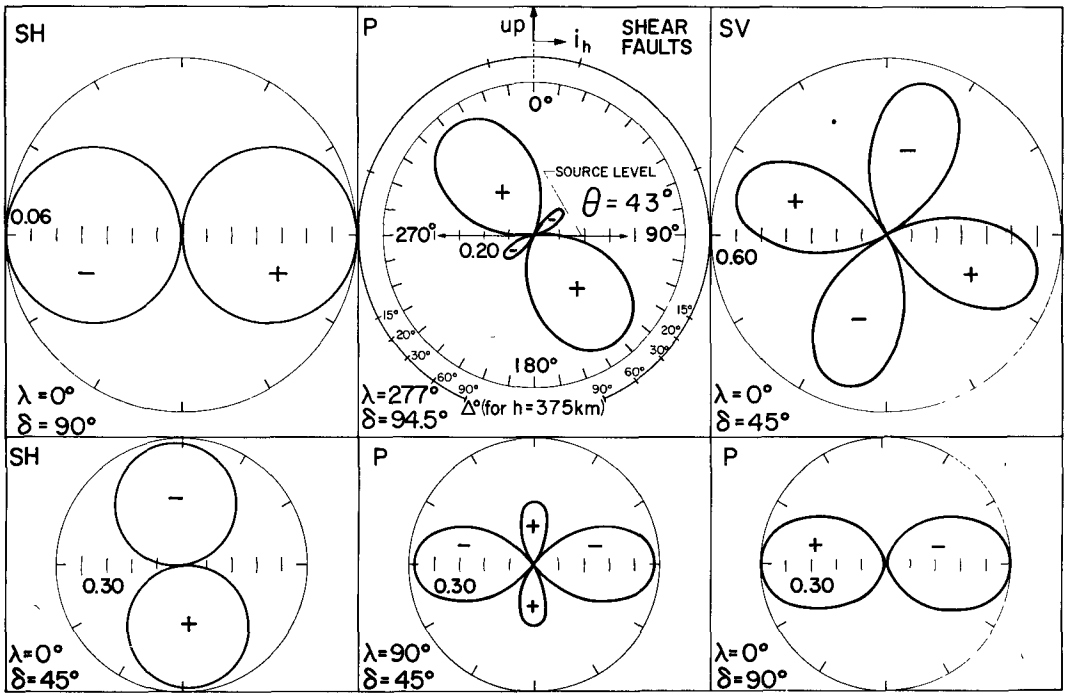

FIG. 17. Vertical radiation patterns of the far field of body waves in a boundless elastic medium.

must first extend previous theoretical results obtained by Ben-Menahem (1962) for the finiteness factors of strike slip motion. Following the same procedure given therein we consider a uniform rupture in the direction of the displacement vector. Expanding the travel-time along the ray into Taylor series about the point-source

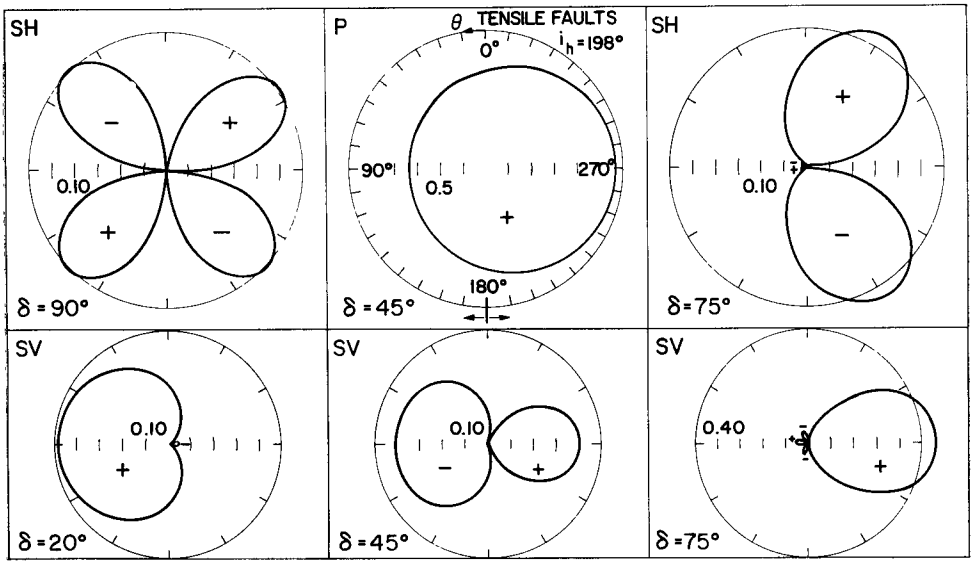

FIG. 18. Horizontal radiation patterns of the far field of body waves in a boundless elastic medium due to tensile faults.

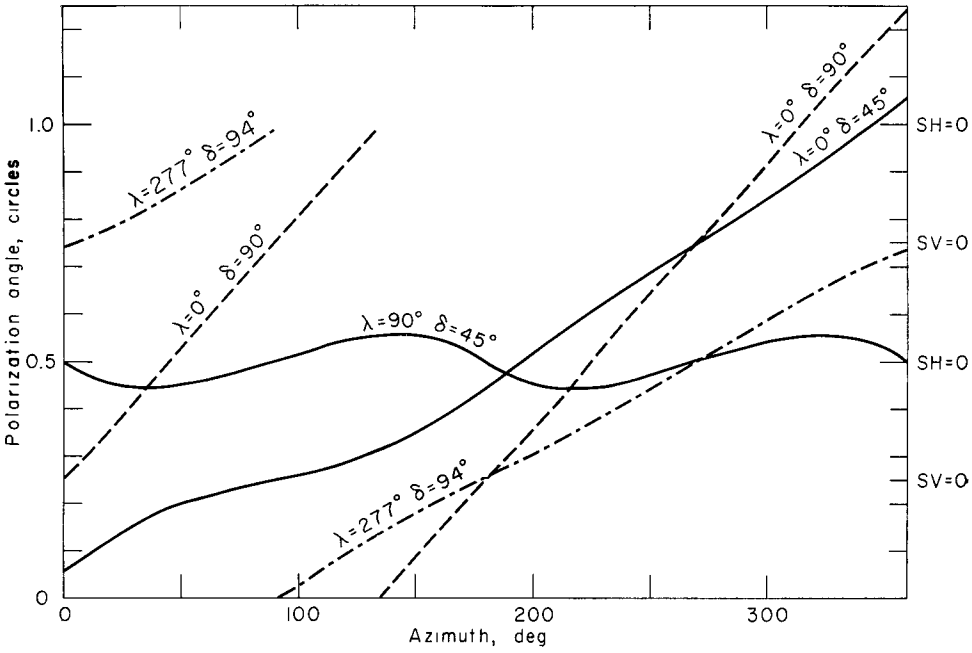

FIG. 19. Examples illustrating the dependence of the polarization angle on the azimuth (counterclockwise from strike of fault) and the fault parameters.

TABLE 6

VERTICAL RADIATION PATTERNS FOR THE FAR FIELD OF BODY WAVES DUE TO A SHEAR FAULT (AN EXAMPLE). POLARIZATION ϵ IS GIVEN BOTH IN DEGREES AND CIRCLES IN THE TWO RIGHT COLUMNS

THETA = 223.DEGREE
LAMBDA = 60.DEGREE DELTA = 55.DEGREE

I(N)(DEG)	P	SH	SV	E(DEG)	E(POC)
0.	0.132	0.408	-0.014	91.949	0.255
5.0	0.125	0.369	-0.153	112.523	0.313
10.0	0.105	0.326	-0.287	131.352	0.365
15.0	0.075	0.282	-0.413	145.708	0.405
20.0	0.034	0.235	-0.526	155.961	0.433
25.0	-0.017	0.186	-0.623	163.390	0.454
30.0	-0.075	0.136	-0.701	169.047	0.470
35.0	-0.138	0.085	-0.758	173.639	0.482
40.0	-0.206	0.033	-0.792	177.637	0.493
45.0	-0.276	-0.019	-0.802	181.386	0.504
50.0	-0.345	-0.071	-0.787	185.178	0.514
55.0	-0.413	-0.123	-0.749	189.310	0.526
60.0	-0.475	-0.173	-0.687	194.142	0.539
65.0	-0.532	-0.222	-0.605	200.171	0.556
70.0	-0.581	-0.270	-0.505	208.126	0.578
75.0	-0.620	-0.315	-0.389	219.027	0.608
80.0	-0.648	-0.358	-0.261	233.904	0.650
85.0	-0.665	-0.398	-0.126	252.512	0.701
90.0	-0.670	-0.436	0.014	271.826	0.755
95.0	-0.663	-0.470	0.153	288.035	0.800
100.0	-0.643	-0.500	0.287	299.881	0.833
105.0	-0.613	-0.526	0.413	308.104	0.856
110.0	-0.572	-0.549	0.526	313.771	0.872
115.0	-0.521	-0.567	0.623	317.678	0.882
120.0	-0.463	-0.581	0.701	320.337	0.890
125.0	-0.400	-0.591	0.758	322.059	0.895
130.0	-0.332	-0.596	0.792	323.028	0.897
135.0	-0.262	-0.597	0.802	323.339	0.898
140.0	-0.193	-0.593	0.787	323.017	0.897
145.0	-0.125	-0.584	0.749	322.027	0.895
150.0	-0.063	-0.571	0.687	320.264	0.890
155.0	-0.006	-0.554	0.605	317.524	0.882
160.0	0.043	-0.533	0.505	313.457	0.871
165.0	0.082	-0.507	0.389	307.480	0.854
170.0	0.110	-0.478	0.261	298.665	0.830
175.0	0.127	-0.445	0.126	285.765	0.794
180.0	0.132	-0.408	-0.014	268.051	0.745
185.0	0.125	-0.369	-0.153	247.477	0.687
190.0	0.105	-0.326	-0.287	228.648	0.635
195.0	0.075	-0.282	-0.413	214.292	0.595
200.0	0.034	-0.235	-0.526	204.039	0.567
205.0	-0.017	-0.186	-0.623	196.610	0.546
210.0	-0.075	-0.136	-0.701	190.953	0.530
215.0	-0.138	-0.085	-0.758	186.361	0.518
220.0	-0.206	-0.033	-0.792	182.363	0.507
225.0	-0.276	0.019	-0.802	178.614	0.496
230.0	-0.345	0.071	-0.787	174.822	0.486
235.0	-0.413	0.123	-0.749	170.690	0.474
240.0	-0.475	0.173	-0.687	165.858	0.461
245.0	-0.532	0.222	-0.605	159.829	0.444
250.0	-0.581	0.270	-0.505	151.874	0.422
255.0	-0.620	0.315	-0.389	140.973	0.392
260.0	-0.648	0.358	-0.261	126.097	0.350
265.0	-0.665	0.398	-0.126	107.488	0.299
270.0	-0.670	0.436	0.014	88.174	0.245
275.0	-0.663	0.470	0.153	71.965	0.200
280.0	-0.643	0.500	0.287	60.119	0.167
285.0	-0.613	0.526	0.413	51.896	0.144
290.0	-0.572	0.549	0.526	46.229	0.128
295.0	-0.521	0.567	0.623	42.322	0.118
300.0	-0.463	0.581	0.701	39.663	0.110
305.0	-0.400	0.591	0.758	37.941	0.105
310.0	-0.332	0.596	0.792	36.972	0.103
315.0	-0.262	0.597	0.802	36.661	0.102
320.0	-0.193	0.593	0.787	36.983	0.103
325.0	-0.125	0.584	0.749	37.973	0.105
330.0	-0.063	0.571	0.687	39.736	0.110
335.0	-0.006	0.554	0.605	42.476	0.118
340.0	0.043	0.533	0.505	46.543	0.129
345.0	0.082	0.507	0.389	52.520	0.146
350.0	0.110	0.478	0.261	61.335	0.170
355.0	0.127	0.445	0.126	74.235	0.206

TABLE 7

Vertical Radiation Patterns for the Far Field of Body Waves Due to a Tensile Fault (an Example)

THETA = 223.DEGREE

DELTA = 45.DEGREE

I(KM)I(DEG)	P	SH	SV	E(DEG)	E(POC)
0.	4.511	-0.366	0.341	313.000	0.869
5.0	4.739	-0.386	0.313	309.000	0.858
10.0	4.945	-0.403	0.275	304.251	0.845
15.0	5.121	-0.418	0.228	298.672	0.830
20.0	5.262	-0.429	0.175	292.226	0.812
25.0	5.364	-0.437	0.117	284.965	0.792
30.0	5.424	-0.441	0.055	277.064	0.770
35.0	5.440	-0.443	-0.009	268.832	0.747
40.0	5.412	-0.440	-0.072	260.656	0.724
45.0	5.340	-0.435	-0.134	252.909	0.703
50.0	5.226	-0.426	-0.191	245.866	0.683
55.0	5.075	-0.414	-0.242	239.665	0.666
60.0	4.890	-0.399	-0.286	234.326	0.651
65.0	4.677	-0.381	-0.322	229.798	0.638
70.0	4.443	-0.359	-0.347	225.993	0.628
75.0	4.195	-0.336	-0.362	222.814	0.619
80.0	3.940	-0.309	-0.366	220.169	0.612
85.0	3.686	-0.280	-0.359	217.980	0.606
90.0	3.441	-0.249	-0.341	216.180	0.601
95.0	3.212	-0.217	-0.313	214.715	0.596
100.0	3.007	-0.182	-0.275	213.541	0.593
105.0	2.831	-0.146	-0.228	212.626	0.591
110.0	2.689	-0.109	-0.175	211.944	0.589
115.0	2.587	-0.071	-0.117	211.477	0.587
120.0	2.527	-0.033	-0.055	211.212	0.587
125.0	2.511	0.005	0.009	31.143	0.087
130.0	2.540	0.044	0.072	31.267	0.087
135.0	2.612	0.082	0.134	31.588	0.088
140.0	2.725	0.120	0.191	32.114	0.089
145.0	2.877	0.157	0.242	32.860	0.091
150.0	3.062	0.192	0.286	33.845	0.094
155.0	3.275	0.226	0.322	35.097	0.097
160.0	3.509	0.258	0.347	36.652	0.102
165.0	3.757	0.289	0.362	38.556	0.107
170.0	4.012	0.317	0.366	40.867	0.114
175.0	4.266	0.343	0.359	43.654	0.121
180.0	4.511	0.366	0.341	47.000	0.131
185.0	4.739	0.386	0.313	51.000	0.142
190.0	4.945	0.403	0.275	55.748	0.155
195.0	5.121	0.418	0.228	61.328	0.170
200.0	5.262	0.429	0.175	67.774	0.188
205.0	5.364	0.437	0.117	75.035	0.208
210.0	5.424	0.441	0.055	82.936	0.230
215.0	5.440	0.443	-0.009	91.168	0.253
220.0	5.412	0.440	-0.072	99.344	0.276
225.0	5.340	0.435	-0.134	107.090	0.297
230.0	5.226	0.426	-0.191	114.134	0.317
235.0	5.075	0.414	-0.242	120.335	0.334
240.0	4.890	0.399	-0.286	125.674	0.349
245.0	4.677	0.381	-0.322	130.202	0.362
250.0	4.443	0.359	-0.347	134.007	0.372
255.0	4.195	0.336	-0.362	137.186	0.381
260.0	3.940	0.309	-0.366	139.831	0.388
265.0	3.686	0.280	-0.359	142.020	0.394
270.0	3.441	0.249	-0.341	143.820	0.399
275.0	3.212	0.217	-0.313	145.285	0.404
280.0	3.007	0.182	-0.275	146.459	0.407
285.0	2.831	0.146	-0.228	147.374	0.409
290.0	2.689	0.109	-0.175	148.056	0.411
295.0	2.587	0.071	-0.117	148.523	0.413
300.0	2.527	0.033	-0.055	148.788	0.413
305.0	2.511	-0.005	0.009	328.857	0.913
310.0	2.540	-0.044	0.072	328.733	0.913
315.0	2.612	-0.082	0.134	328.412	0.912
320.0	2.725	-0.120	0.191	327.886	0.911
325.0	2.877	-0.156	0.242	327.140	0.909
330.0	3.062	-0.192	0.286	326.155	0.906
335.0	3.275	-0.226	0.322	324.903	0.903
340.0	3.509	-0.258	0.347	323.348	0.898
345.0	3.757	-0.289	0.362	321.444	0.893
350.0	4.012	-0.317	0.366	319.133	0.886
355.0	4.266	-0.343	0.359	316.346	0.879

*POISSON RATIO = 0.2783 (EVALUATED AT DEPTH = 350 KM)

TABLE 8

HORIZONTAL RADIATION PATTERN FOR THE FAR FIELD OF BODY WAVES DUE TO A TENSILE FAULT (AN EXAMPLE)

I(H) = 198.DEGREE

DELTA = 20.DEGREE

THETA	P	SH	SV	E(DEG)	E(POC)
0.	5.705	0.306	-C.260	130.332	0.362
5.0	5.640	0.301	-C.282	133.090	0.370
10.0	5.576	0.295	-C.304	135.841	0.377
15.0	5.513	0.286	-C.325	138.588	0.385
20.0	5.452	0.276	-C.344	141.333	0.393
25.0	5.394	C.263	-C.363	144.077	0.400
30.0	5.339	0.249	-C.381	146.822	0.408
35.0	5.287	0.233	-C.397	149.570	0.415
40.0	5.238	0.216	-C.412	152.320	0.423
45.0	5.193	C.198	-C.426	155.074	0.431
50.0	5.153	0.179	-C.439	157.831	0.438
55.0	5.116	0.158	-C.449	160.592	0.446
60.0	5.085	0.137	-C.459	163.357	0.454
65.0	5.057	0.115	-C.467	166.125	0.461
70.0	5.035	0.093	-C.473	168.896	0.469
75.0	5.017	0.070	-C.479	171.670	0.477
80.0	5.005	0.047	-C.482	174.446	0.485
85.0	4.997	0.024	-C.484	177.222	0.492
90.0	4.994	0.000	-C.485	180.000	0.500
95.0	4.997	-0.024	-C.484	182.778	0.508
100.0	5.005	-0.047	-C.482	185.554	0.515
105.0	5.017	-0.070	-C.479	188.330	0.523
110.0	5.035	-0.093	-C.473	191.104	0.531
115.0	5.057	-0.115	-C.467	193.875	0.539
120.0	5.085	-0.137	-C.459	196.643	0.546
125.0	5.116	-0.158	-C.449	199.408	0.554
130.0	5.153	-0.179	-C.439	202.169	0.562
135.0	5.193	-0.198	-C.426	204.926	0.569
140.0	5.238	-0.216	-C.412	207.680	0.577
145.0	5.287	-0.233	-C.397	210.430	0.585
150.0	5.339	-0.249	-C.381	213.178	0.592
155.0	5.394	-0.263	-C.363	215.923	0.600
160.0	5.452	-0.276	-C.344	218.667	0.607
165.0	5.513	-0.286	-C.325	221.412	0.615
170.0	5.576	-0.295	-C.304	224.159	0.623
175.0	5.640	-0.301	-C.282	226.910	0.630
180.0	5.705	-0.306	-C.260	229.668	0.638
185.0	5.772	-0.308	-C.237	232.438	0.646
190.0	5.838	-0.307	-C.213	235.223	0.653
195.0	5.904	-0.304	-C.190	238.030	0.661
200.0	5.969	-0.299	-C.167	240.867	0.669
205.0	6.033	-0.291	-C.143	243.743	0.677
210.0	6.094	-0.280	-C.121	246.671	0.685
215.0	6.154	-0.267	-C.099	249.669	0.694
220.0	6.210	-0.252	-C.078	252.762	0.702
225.0	6.262	-0.234	-C.058	255.983	0.711
230.0	6.310	-0.214	-C.040	259.385	0.721
235.0	6.354	-0.192	-C.023	263.046	0.731
240.0	6.393	-0.168	-0.009	267.094	0.742
245.0	6.427	-0.143	C.004	271.753	0.755
250.0	6.455	-0.116	C.015	277.443	0.771
255.0	6.477	-0.088	C.024	285.058	0.792
260.0	6.493	-0.059	C.030	296.767	0.824
265.0	6.503	-0.030	C.034	318.473	0.885
270.0	6.506	-0.000	C.035	360.000	1.000
275.0	6.503	0.030	C.034	41.526	0.115
280.0	6.493	0.059	C.030	63.233	0.176
285.0	6.477	C.088	C.024	74.942	C.208
290.0	6.455	0.116	C.015	82.557	0.229
295.0	6.427	0.143	C.004	88.247	0.245
300.0	6.393	0.168	-C.009	92.906	0.258
305.0	6.354	0.192	-C.023	96.954	0.269
310.0	6.310	0.214	-0.040	100.615	0.279
315.0	6.262	0.234	-C.058	104.017	0.289
320.0	6.210	0.252	-C.078	107.238	0.298
325.0	6.154	0.267	-C.099	110.331	0.306
330.0	6.094	0.280	-0.121	113.329	0.315
335.0	6.033	0.291	-C.143	116.257	0.323
340.0	5.969	0.299	-C.167	119.133	0.331
345.0	5.904	0.304	-C.190	121.970	0.339
350.0	5.838	0.307	-C.213	124.777	0.347
355.0	5.772	0.308	-C.237	127.562	0.354

*POISSON RATIO = 0.2783 (EVALUATED AT DEPTH = 350 KM)

TABLE 9

HORIZONTAL RADIATION PATTERN FOR THE FAR FIELD OF BODY WAVES DUE TO A SHEAR FAULT (AN EXAMPLE)

I(H) = 70.DEGREE

LAMBDA = 60.DEGREE DELTA = 55.DEGREE

THETA	P	SH	SV	E(DEG)	E(POC)
0.	0.140	-0.483	-0.483	224.949	0.625
5.0	0.098	-0.552	-0.488	228.495	0.635
10.0	0.050	-0.606	-0.494	230.802	0.641
15.0	-0.001	-0.645	-0.502	232.124	0.645
20.0	-0.055	-0.667	-0.509	232.636	0.646
25.0	-0.110	-0.672	-0.517	232.444	0.646
30.0	-0.165	-0.659	-0.522	231.599	0.643
35.0	-0.218	-0.629	-0.526	230.104	0.639
40.0	-0.267	-0.584	-0.527	227.914	0.633
45.0	-0.313	-0.523	-0.525	224.932	0.625
50.0	-0.353	-0.450	-0.518	220.997	0.614
55.0	-0.386	-0.367	-0.507	215.874	0.600
60.0	-0.413	-0.275	-0.492	209.246	0.581
65.0	-0.431	-0.178	-0.471	200.743	0.558
70.0	-0.442	-0.079	-0.446	190.069	0.528
75.0	-0.444	0.020	-0.416	177.305	0.493
80.0	-0.439	0.115	-0.382	163.246	0.453
85.0	-0.426	0.204	-0.344	149.305	0.415
90.0	-0.406	0.285	-0.303	136.781	0.380
95.0	-0.379	0.355	-0.260	126.246	0.351
100.0	-0.348	0.412	-0.215	117.625	0.327
105.0	-0.312	0.454	-0.170	110.562	0.307
110.0	-0.274	0.482	-0.126	104.662	0.291
115.0	-0.234	0.493	-0.083	99.586	0.277
120.0	-0.193	0.488	-0.043	95.057	0.264
125.0	-0.154	0.468	-0.007	90.847	0.252
130.0	-0.117	0.432	0.025	86.738	0.241
135.0	-0.083	0.384	0.051	82.490	0.229
140.0	-0.054	0.323	0.070	77.761	0.216
145.0	-0.031	0.254	0.083	71.931	0.200
150.0	-0.013	0.177	0.088	63.551	0.177
155.0	-0.002	0.095	0.085	48.127	0.134
160.0	0.003	0.012	0.075	8.949	0.025
165.0	0.000	-0.071	0.057	308.696	0.857
170.0	-0.009	-0.149	0.031	281.653	0.782
175.0	-0.024	-0.221	-0.002	269.468	0.749
180.0	-0.045	-0.285	-0.041	261.747	0.727
185.0	-0.071	-0.337	-0.086	255.662	0.710
190.0	-0.100	-0.377	-0.136	250.186	0.695
195.0	-0.132	-0.403	-0.189	244.835	0.680
200.0	-0.166	-0.414	-0.245	239.328	0.665
205.0	-0.200	-0.409	-0.303	233.477	0.649
210.0	-0.232	-0.389	-0.361	227.150	0.631
215.0	-0.263	-0.354	-0.418	220.269	0.612
220.0	-0.290	-0.305	-0.473	212.829	0.591
225.0	-0.313	-0.244	-0.525	204.912	0.569
230.0	-0.330	-0.172	-0.573	196.700	0.546
235.0	-0.341	-0.092	-0.616	188.457	0.523
240.0	-0.345	-0.005	-0.654	180.474	0.501
245.0	-0.341	0.084	-0.686	173.012	0.481
250.0	-0.331	0.174	-0.711	166.251	0.462
255.0	-0.313	0.261	-0.729	160.283	0.445
260.0	-0.288	0.344	-0.741	155.126	0.431
265.0	-0.257	0.418	-0.747	150.754	0.419
270.0	-0.220	0.482	-0.746	147.118	0.409
275.0	-0.178	0.534	-0.740	144.170	0.400
280.0	-0.133	0.572	-0.728	141.870	0.394
285.0	-0.085	0.594	-0.713	140.198	0.389
290.0	-0.036	0.599	-0.693	139.158	0.387
295.0	0.013	0.588	-0.671	138.786	0.386
300.0	0.060	0.560	-0.648	139.155	0.387
305.0	0.105	0.516	-0.623	140.391	0.390
310.0	0.145	0.456	-0.599	142.686	0.396
315.0	0.179	0.383	-0.575	146.313	0.406
320.0	0.207	0.299	-0.553	151.626	0.421
325.0	0.228	0.205	-0.533	158.997	0.442
330.0	0.241	0.104	-0.516	168.610	0.468
335.0	0.245	-0.001	-0.503	180.081	0.500
340.0	0.240	-0.107	-0.492	192.213	0.534
345.0	0.227	-0.210	-0.485	203.451	0.565
350.0	0.206	-0.310	-0.482	212.738	0.591
355.0	0.177	-0.401	-0.481	219.823	0.611

arrival time,

$$t_p(\Delta; R) = t_p(\Delta_0; R_0) + (\delta\Delta)\frac{\partial t}{\partial \Delta} + (\delta R)\frac{\partial t}{\partial R} + \cdots \tag{30}$$

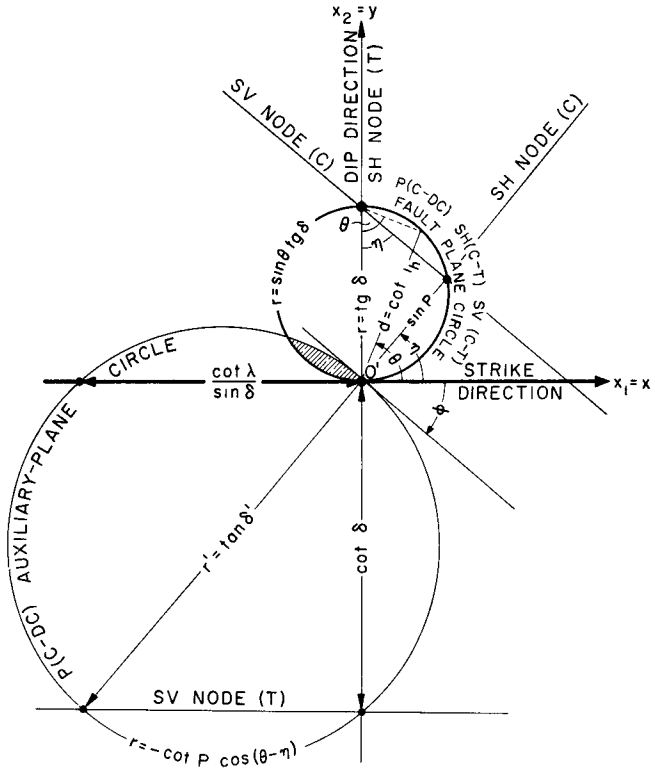

FIG. 20. Nodal lines on Byerly's extended distance projection plane. *P(C-DC)* P waves due to couple and double couple *SH(C-T)* *SH* waves due to couple and tensile fault.

and making use of the relations

$$\begin{aligned} h &= a - R_0 \\ \frac{\partial t_p}{\partial \Delta} &= \frac{\sin i_0}{v(a)} \qquad \frac{\partial t_p}{\partial R} = -\frac{\cos i_h}{v(h)} \end{aligned} \tag{31}$$

We finally obtain a finiteness factor for a shear fault in the form $\sin x/xe^{-ix}$, where

$$x = \frac{\omega b}{2V_a}\left\{\frac{V_a}{V_f} - |\cos p|\cos(\theta - \eta) - \sin p \cot i_h\right\} \tag{32}$$

As before b is the fault-length in the direction of rupture, V_a is the apparent body wave velocity (phase velocity) at the surface, p is the plunge angle of the displace-

ment vector and η is the azimuth of trend, defined by

$$\sin p = \sin \lambda \sin \delta$$

$$\cos \eta = \frac{\cos \lambda}{\sqrt{1 - \sin^2 \lambda \sin^2 \delta}} \tag{33}$$

For a strike-slip fault $p = 0$ $\eta = 0$ and equation (32) reduces to the form $x = (\omega b/2V_a)(V_a/V_f - \cos \theta)$. Note that we have assumed quite arbitrarily that the rupture is progressing in the direction of the initial displacement vector. If the fault propagates in an independent direction, equation (32) will still be valid, provided that the angles p and η are replaced.

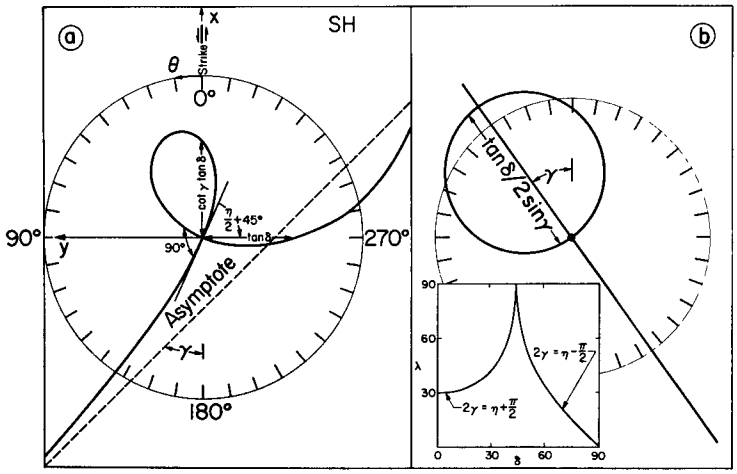

FIG. 21. Nodal lines on the extended distance projection plane for *SH* waves due to shear faults (double couple) Equation of nodals:

$$(x^2 + y^2)(x \sin \lambda \cos 2\delta - y \cos \lambda \cos \delta) = xy \sin \lambda \sin 2\delta + (x^2 - y^2) \cos \lambda \cos \delta$$

Note also that for P and S waves at distances $\Delta > 70°$ and plunge angles $p > 30°$, the finiteness parameter will be approximately equal to $x = \omega b/2V_f$. In most cases the finiteness factor will depend only slightly on the azimuth. Moreover, due to the linear dependence of x on the frequency, the effect of the finiteness on the spectrums will be equivalent to that of a filter with a box-car impulse response, the length of this box-car being equal to the time of rupture.

5. *Nodal Curves*

In Byerly's method one obtains the nodal curves from the sign distribution of the first motion. The body wave spectrums preserve these curves without change, at least to the extent that the angle of emergence i_h is frequency independent. A propagating rupture may, in principle, introduce an additional nodal curve which is frequency dependent. Nodal curves for a couple relative to a shear fault (λ; δ) and a dipping tensile fault are shown together in Figure 20. Nodal curves of *SH* due to a shear fault can be put in the form

$$\cot i_h = \frac{\cos 2\theta \cos \lambda + \sin 2\theta \sin \lambda \cos \delta}{\cos \theta \sin \lambda \cos 2\delta - \sin \theta \cos \lambda \cos \delta} \sin \delta$$

$$= \left[\frac{\cos \gamma}{\cos \eta}\right] \frac{\cos (2\theta - \eta)}{\sin (\gamma - \theta)} \tan \delta \qquad (34)$$

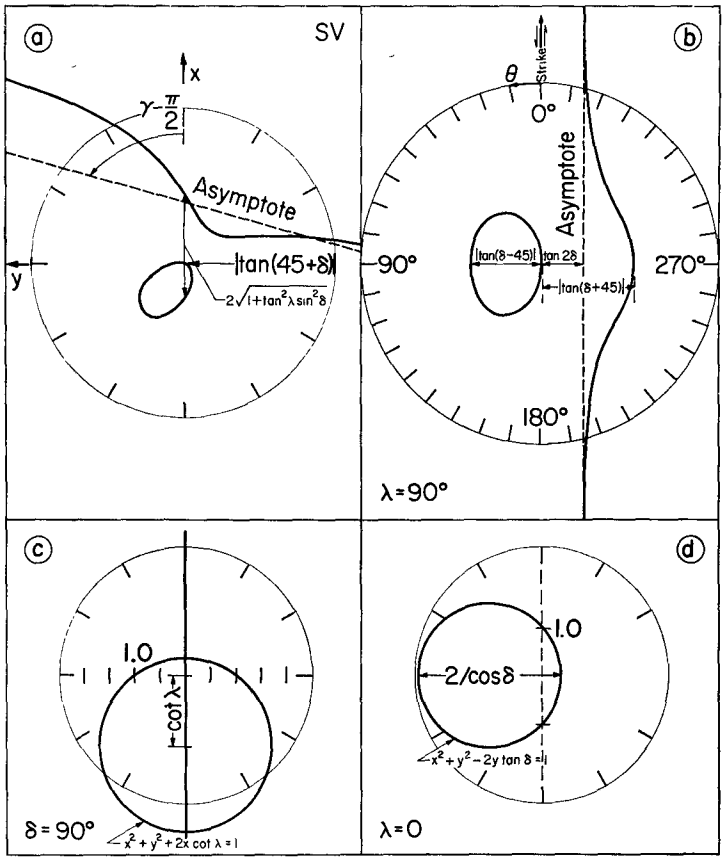

FIG. 22. Nodal lines on the extended distance projection plane for *SV* waves due to shear faults (double couple) Equation of nodals:

$$(y \sin \lambda \cos 2\delta + x \cos \lambda \cos \delta)(x^2 + y^2 - 1) = 2xy \cos \lambda \sin \delta + \sin \lambda \sin 2\delta (x^2 + 2y^2)$$

The curves can be classified in three groups:

1. *Typical*: (Figure 21[a]) The nodal curve is a strophoid which divides the plane of projection into three sections. This curve corresponds to downgoing rays only ($270° \geqq i_h \geqq 90°$). The nodal curve for the upgoing rays ($|\, i_h \,| < 90°$) is obtained from the one shown in Figure 21[a], by a reflection around a line parallel to the asymptote through the origin. This is an immediate consequence of the symmetry relations given in equation (22).

2. *Atypical*: For particular combinations of δ and λ ($\eta/2 = \gamma \pm 45°$) the nodal curves reduce to a circle with a bisecting straight line (Figure 21). The points in the (λ; δ) plane for which this reduction is possible are shown in the same figure.

Here again one obtains the reflected circle $r = -\tan\delta\cdot\cos(\theta-\gamma)/2\sin\gamma$ for the upgoing rays, $|i_h| < 90°$.

TABLE 10

NODAL LINES ON THE EXTENDED DISTANCE PROJECTION PLANE FOR A SHEAR TYPE FAULT $\delta = 61°$, $\lambda = 28°$ (AN EXAMPLE)

THETA	SH	SV	THETA	SH	SV	THETA	SH	SV	THETA	SH	SV	THETA	SH	SV	THETA	SH	SV
0.	-4.058	1.568	60.0	0.564	0.001	120.0	2.964	0.968	180.0	4.058	0.638	240.0	-0.564	961.828	300.0	-2.964	1.033
1.0	-3.973	1.621	61.0	0.635	0.007	121.0	2.947	0.990	181.0	3.973	0.617	241.0	-0.635	134.954	301.0	-2.947	1.010
2.0	-3.890	1.676	62.0	0.705	0.014	122.0	2.926	1.011	182.0	3.890	0.597	242.0	-0.705	72.148	302.0	-2.926	0.989
3.0	-3.807	1.735	63.0	0.774	0.020	123.0	2.901	1.031	183.0	3.867	0.577	243.0	-0.774	49.014	303.0	-2.901	0.970
4.0	-3.726	1.796	64.0	0.843	0.027	124.0	2.871	1.051	184.0	3.726	0.557	244.0	-0.843	36.973	304.0	-2.871	0.952
5.0	-3.645	1.860	65.0	0.912	0.034	125.0	2.836	1.069	185.0	3.645	0.538	245.0	-0.912	29.580	305.0	-2.836	0.935
6.0	-3.565	1.927	66.0	0.979	0.041	126.0	2.796	1.087	186.0	3.565	0.519	246.0	-0.979	24.574	306.0	-2.796	0.920
7.0	-3.485	1.998	67.0	1.046	0.048	127.0	2.750	1.104	187.0	3.485	0.500	247.0	-1.046	20.956	307.0	-2.750	0.906
8.0	-3.406	2.072	68.0	1.113	0.055	128.0	2.697	1.119	188.0	3.406	0.483	248.0	-1.113	18.215	308.0	-2.697	0.893
9.0	-3.328	2.149	69.0	1.179	0.062	129.0	2.637	1.134	189.0	3.328	0.465	249.0	-1.179	16.065	309.0	-2.637	0.882
10.0	-3.249	2.230	70.0	1.244	0.070	130.0	2.569	1.148	190.0	3.249	0.448	250.0	-1.244	14.332	310.0	-2.569	0.871
11.0	-3.171	2.315	71.0	1.308	0.078	131.0	2.491	1.160	191.0	3.171	0.432	251.0	-1.308	12.903	311.0	-2.491	0.862
12.0	-3.093	2.404	72.0	1.371	0.086	132.0	2.403	1.172	192.0	3.093	0.416	252.0	-1.371	11.704	312.0	-2.403	0.853
13.0	-3.016	2.496	73.0	1.434	0.094	133.0	2.301	1.182	193.0	3.016	0.401	253.0	-1.434	10.683	313.0	-2.301	0.846
14.0	-2.938	2.593	74.0	1.496	0.102	134.0	2.186	1.191	194.0	2.938	0.386	254.0	-1.496	9.803	314.0	-2.186	0.839
15.0	-2.861	2.694	75.0	1.557	0.111	135.0	2.053	1.199	195.0	2.861	0.371	255.0	-1.557	9.034	315.0	-2.053	0.834
16.0	-2.783	2.800	76.0	1.618	0.120	136.0	1.899	1.206	196.0	2.783	0.357	256.0	-1.618	8.358	316.0	-1.899	0.829
17.0	-2.706	2.910	77.0	1.677	0.129	137.0	1.720	1.212	197.0	2.706	0.344	257.0	-1.677	7.758	317.0	-1.720	0.825
18.0	-2.629	3.026	78.0	1.735	0.138	138.0	1.509	1.217	198.0	2.629	0.330	258.0	-1.735	7.221	318.0	-1.510	0.822
19.0	-2.551	3.147	79.0	1.793	0.148	139.0	1.259	1.221	199.0	2.551	0.318	259.0	-1.793	6.738	319.0	-1.259	0.819
20.0	-2.474	3.273	80.0	1.850	0.159	140.0	0.957	1.223	200.0	2.474	0.306	260.0	-1.850	6.302	320.0	-0.958	0.818
21.0	-2.397	3.405	81.0	1.905	0.169	141.0	0.587	1.225	201.0	2.397	0.294	261.0	-1.905	5.904	321.0	-0.587	0.817
22.0	-2.319	3.544	82.0	1.960	0.180	142.0	0.123	1.225	202.0	2.319	0.282	262.0	-1.960	5.542	322.0	-0.123	0.816
23.0	-2.242	3.689	83.0	2.014	0.192	143.0	-0.477	1.224	203.0	2.242	0.271	263.0	-2.014	5.209	323.0	0.477	0.817
24.0	-2.165	3.841	84.0	2.066	0.204	144.0	-1.281	1.222	204.0	2.165	0.260	264.0	-2.066	4.904	324.0	1.280	0.818
25.0	-2.087	4.001	85.0	2.118	0.216	145.0	-2.414	1.219	205.0	2.087	0.250	265.0	-2.118	4.621	325.0	2.413	0.820
26.0	-2.010	4.169	86.0	2.168	0.229	146.0	-4.133	1.215	206.0	2.010	0.240	266.0	-2.168	4.360	326.0	4.133	0.823
27.0	-1.932	4.346	87.0	2.217	0.243	147.0	-7.058	1.209	207.0	1.932	0.230	267.0	-2.217	4.118	327.0	7.057	0.827
28.0	-1.855	4.533	88.0	2.266	0.257	148.0	-13.156	1.203	208.0	1.855	0.221	268.0	-2.266	3.893	328.0	13.154	0.831
29.0	-1.778	4.730	89.0	2.313	0.272	149.0	-33.815	1.196	209.0	1.778	0.211	269.0	-2.313	3.683	329.0	33.803	0.836
30.0	-1.700	4.938	90.0	2.358	0.287	150.0	196.713	1.188	210.0	1.700	0.203	270.0	-2.358	3.487	330.0	197.030	0.842
31.0	-1.623	5.159	91.0	2.403	0.303	151.0	31.237	1.178	211.0	1.623	0.194	271.0	-2.403	3.305	331.0	-31.244	0.849
32.0	-1.545	5.394	92.0	2.446	0.319	152.0	18.653	1.168	212.0	1.545	0.185	272.0	-2.446	3.134	332.0	-18.655	0.856
33.0	-1.468	5.643	93.0	2.488	0.336	153.0	14.008	1.157	213.0	1.468	0.177	273.0	-2.488	2.974	333.0	-14.009	0.864
34.0	-1.390	5.910	94.0	2.529	0.354	154.0	11.583	1.145	214.0	1.390	0.169	274.0	-2.529	2.824	334.0	-11.584	0.874
35.0	-1.313	6.195	95.0	2.568	0.373	155.0	10.087	1.132	215.0	1.313	0.161	275.0	-2.568	2.684	335.0	-10.088	0.884
36.0	-1.235	6.502	96.0	2.606	0.392	156.0	9.068	1.118	216.0	1.235	0.154	276.0	-2.606	2.553	336.0	-9.068	0.895
37.0	-1.158	6.832	97.0	2.642	0.412	157.0	8.325	1.103	217.0	1.158	0.146	277.0	-2.642	2.429	337.0	-8.326	0.907
38.0	-1.081	7.190	98.0	2.677	0.432	158.0	7.757	1.088	218.0	1.081	0.139	278.0	-2.677	2.314	338.0	-7.757	0.919
39.0	-1.004	7.578	99.0	2.711	0.453	159.0	7.306	1.071	219.0	1.004	0.132	279.0	-2.711	2.206	339.0	-7.306	0.933
40.0	-0.927	8.001	100.0	2.742	0.475	160.0	6.937	1.054	220.0	0.927	0.125	280.0	-2.742	2.104	340.0	-6.937	0.948
41.0	-0.850	8.465	101.0	2.773	0.498	161.0	6.627	1.037	221.0	0.850	0.118	281.0	-2.773	2.009	341.0	-6.627	0.965
42.0	-0.773	8.977	102.0	2.801	0.521	162.0	6.362	1.019	222.0	0.773	0.111	282.0	-2.801	1.920	342.0	-6.362	0.982
43.0	-0.696	9.545	103.0	2.828	0.545	163.0	6.132	1.000	223.0	0.696	0.105	283.0	-2.828	1.837	343.0	-6.132	1.000
44.0	-0.620	10.180	104.0	2.854	0.569	164.0	5.928	0.980	224.0	0.620	0.098	284.0	-2.854	1.758	344.0	-5.928	1.020
45.0	-0.544	10.894	105.0	2.877	0.593	165.0	5.746	0.960	225.0	0.544	0.092	285.0	-2.877	1.686	345.0	-5.746	1.041
46.0	-0.468	11.707	106.0	2.899	0.618	166.0	5.580	0.940	226.0	0.468	0.085	286.0	-2.899	1.617	346.0	-5.581	1.064
47.0	-0.392	12.639	107.0	2.919	0.644	167.0	5.429	0.919	227.0	0.392	0.079	287.0	-2.919	1.554	347.0	-5.429	1.088
48.0	-0.316	13.722	108.0	2.936	0.669	168.0	5.289	0.898	228.0	0.316	0.073	288.0	-2.936	1.494	348.0	-5.289	1.113
49.0	-0.241	14.997	109.0	2.952	0.695	169.0	5.159	0.877	229.0	0.241	0.067	289.0	-2.952	1.439	349.0	-5.159	1.141
50.0	-0.166	16.523	110.0	2.966	0.721	170.0	5.037	0.855	230.0	0.166	0.061	290.0	-2.966	1.387	350.0	-5.037	1.169
51.0	-0.091	18.384	111.0	2.977	0.747	171.0	4.921	0.833	231.0	0.091	0.054	291.0	-2.977	1.339	351.0	-4.921	1.200
52.0	-0.017	20.711	112.0	2.986	0.773	172.0	4.811	0.811	232.0	0.017	0.048	292.0	-2.986	1.294	352.0	-4.811	1.232
53.0	0.057	23.705	113.0	2.993	0.798	173.0	4.706	0.789	233.0	-0.057	0.042	293.0	-2.993	1.253	353.0	-4.706	1.267
54.0	0.131	27.711	114.0	2.998	0.824	174.0	4.605	0.767	234.0	-0.131	0.036	294.0	-2.998	1.214	354.0	-4.605	1.303
55.0	0.204	33.358	115.0	2.999	0.849	175.0	4.508	0.745	235.0	-0.204	0.030	295.0	-2.999	1.178	355.0	-4.508	1.341
56.0	0.277	41.926	116.0	2.998	0.874	176.0	4.413	0.724	236.0	-0.277	0.024	296.0	-2.998	1.144	356.0	-4.413	1.382
57.0	0.350	56.510	117.0	2.995	0.898	177.0	4.321	0.702	237.0	-0.350	0.018	297.0	-2.995	1.113	357.0	-4.321	1.425
58.0	0.422	86.937	118.0	2.988	0.922	178.0	4.232	0.680	238.0	-0.422	0.012	298.0	-2.988	1.084	358.0	-4.232	1.470
59.0	0.493	190.097	119.0	2.978	0.945	179.0	4.144	0.659	239.0	-0.493	0.005	299.0	-2.978	1.058	359.0	-4.144	1.518

3. *Singular*: For $\lambda = 90°$ and $\delta \neq 45°$N the nodal curve consists of the line $\theta = \pi/2$ and the circle $r = \tan 2\delta \sin\theta$ which is obtained from the atypical case in the limit $\eta = \gamma \to \pi/2$. The four cases: $\delta = 0$; $\lambda = 90°$ $\delta = 90°$; $\lambda = 90°$ $\delta = 45°$; $\lambda = 0$ $\delta = 90°$ produce nodes which do not depend on i_h.

For SV we find,

$$2\cot 2i_h = \frac{\sin 2\theta\cos\lambda + \sin\lambda\cos\delta\,(3-\cos 2\theta)}{\sin\theta\sin\lambda\cos 2\delta + \cos\lambda\cos\delta\cos\theta}\sin\delta$$

$$= \left\{\frac{\cos\gamma\tan\delta}{\cos\eta}\right\}\frac{\sin(2\theta-\eta)+3\sin\eta}{\cos(\theta-\gamma)} \qquad (35)$$

The nodal curves can be arranged in two groups:

1. *Typical*: ($\lambda \neq 45°$N; $\delta \neq 45°$N) Nodals consist of an open curve having an asymptote at ($\theta = \gamma - 90°$) and a closed line passing through the origin (Figure 22[a]). Nodals for upgoing rays and downgoing rays do coincide.

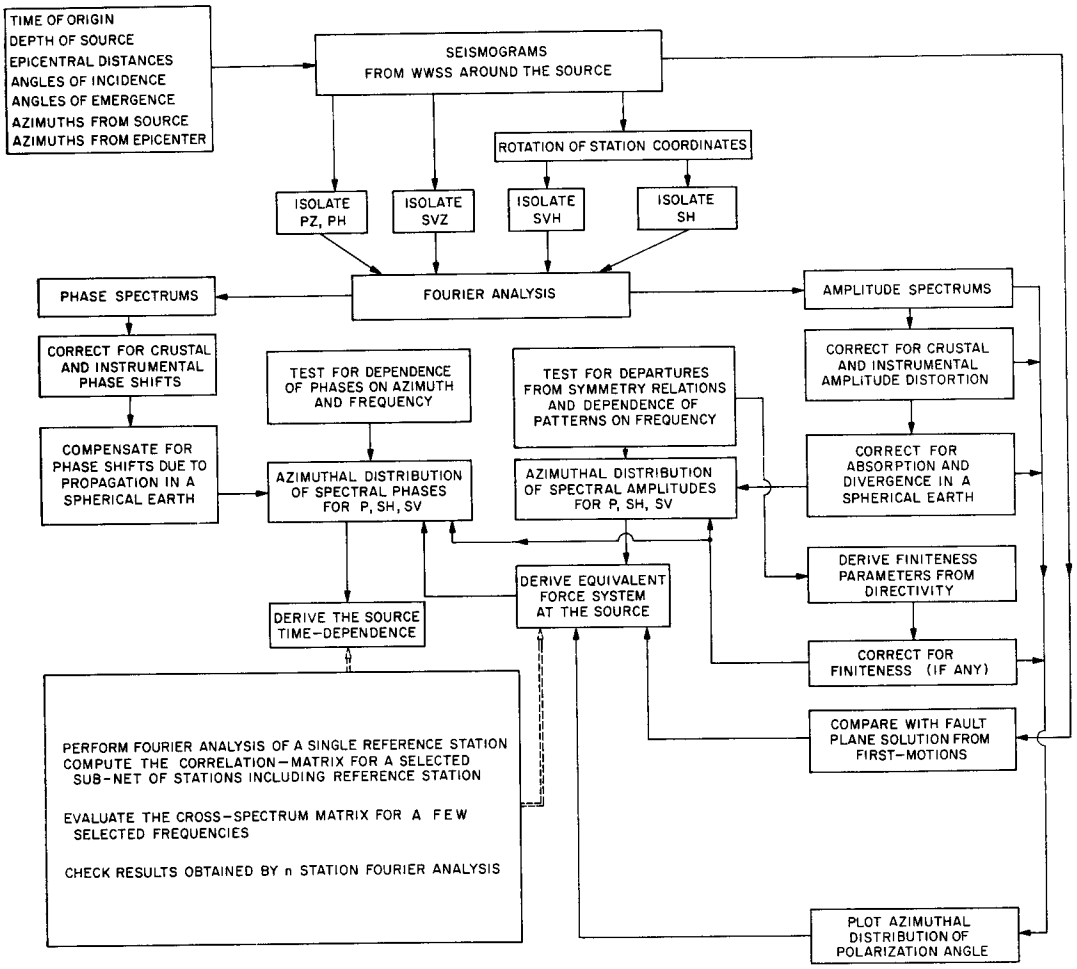

FIG. 23. Data processing scheme for source studies of deep shocks from spectrums of isolated body-wave pulses.

2. *Singular*: For $\delta = 90°$ (Figure 22[c]) and $\lambda = 0$ (Fig. 22[d]) they reduce to lines and circles. For $\lambda = 90°$ (Figure 22[b]) one obtains a tiny closed curve on one side of the strike and an open curve on the other side.

Table 10 shows a computer print-out of the *SH* and *SV* nodals for a shear fault with arbitrary elements.

CONCLUSION

A flow-diagram (Figure 23) summarizes the procedure which we have outlined throughout this paper. In addition we suggest at the lower left corner of this dia-

gram, an alternative method that uses correlation technique and power spectrums instead or in conjunction with the conventional Fourier analysis.

Studies of source mechanism began at the high frequency end of the seismic spectrum (initial motion). It then shifted to the low frequency end (surface waves, free oscillations). The time is ripe now to close the gap and explore the mid-frequency range. In the context of the present paper we have shown that such a project is feasible and that source information can be extracted from the spectrums of P and S waves in the period range 10–100 sec. We believe that similar technique can be devised for any isolated pulse on the seismogram.

Acknowledgments

This research was supported by contract No. AF-49(638)-1337 of the Air Force Office of Scientific Research as part of the Advanced Research Projects Agency Project Vela and by AF-AFOSR 62-421. Discussions held with Dr. Robert Burridge are gratefully acknowledged.

References

Aki, K., and F. Press
1961. "Upper mantle structure under oceans and continents from Rayleigh waves," *J. Royal Astron. Soc.*, 5: 292–305.

Aki, K.
1961. "Crustal structure in Japan from the phase velocity of Rayleigh waves," *Bull. Earthquake Res. Inst. Tokyo Univ.*, 39: 255–283.

Aki, K.
1960. "Study of earthquake mechanism by a method of phase equalization applied to Rayleigh and Love waves," *J. Geophys. Res.*, 65: 729–740.

Anderson, D. L., and C. B. Archambeau
1964. "The anelasticity of the earth," *J. Geophys. Res.*, 69: 2071–2084.

Anderson, Don L., Ari Ben-Menahem and Charles B. Archambeau
1965. Attenuation of seismic energy in the upper mantle, *Journ. of Geophys. Res.* (in press).

Ben-Menahem, A.
1962. "Radiation of seismic body waves from a finite moving source in the earth," *J. Geophys. Res.*, 67: 345–350.

Ben-Menahem, A., and M. N. Toksöz
1963. "Source mechanism from spectra of long-period surface waves, 2. The Kamchatka earthquake of November 4, 1952," *J. Geophys. Res.*, 68: 5207–5222.

Ben-Menahem, A.
1964. "Mode ray duality," *Bull. Seismol. Soc. Am.*, 54: 1315–1321.

Ben-Menahem, A.
1964. "Spectral response of an elastic sphere to dipolar point sources," *Bull. Seismol. Soc. Am.*, 54: 1323–1340.

Ben-Menahem, A., and D. G. Harkrider
1964. "Radiation patterns of seismic surface waves from buried dipolar point sources in a flat stratified earth," *J. Geophys. Res.*, 69: 2605–2620.

Bremmer, H.
1949. "Terrestrial radio waves," Elsevier Publishing Co., New York.

Brune, J. N.
1964. "Travel times, body waves and dispersion in the earth," Abstracts of papers submitted to the annual meeting of the Seismol. Soc. Am., Seattle, Washington, March 27–28.

Brune, J. N.
1964. "Travel times, body waves and normal modes of the earth," *Bull. Seismol. Soc. Am.*, 54: 2099–2128.

Bullen, K. E.
1953. "An Introduction to the Theory of Seismology," Cambridge Univ. Press.
Byerly, P.
1926. "The Montana earthquake of June 28, 1925, G.M.C.T.," *Bull. Seismol. Soc. Am.*, 16: 209–265.
Gilbert, F., and G. J. F. MacDonald
1960. "Free oscillations of the earth, 1. Toroidal oscillations," *J. Geophys. Res.*, 65: 675–693.
Gutenberg, B.
1952. "*SV* and *SH*," Trans. Am. Geophys. Union, 33: 573–584.
Haskell, N. A.
1962. "Crustal reflection of plane *P* and *SV* waves," *J. Geophys. Res.*, 67: 4751–4767.
Haskell, N. A.
1964. "Total energy and energy spectral density of elastic wave radiation from propagating faults," *Bull. Seismol. Soc. Am.*, (in press).
Healy, J. H.
1963. "Crustal structure along the coast of California from seismic refraction measurements," *J. Geophys. Res.*, 68: 5777–5787.
Jackson, W. H., S. W. Stewart and L. C. Pakiser
1963. "Crustal structure in Eastern Colorado from seismic refraction measurements," *J. Geophys. Res.*, 68: 5767–5776.
Jeffreys, H.
1926. "On the amplitudes of bodily seismic waves," *Monthly Notices Roy. Astron. Soc. Geophys. Suppl. 1*, 334–348.
Karal, F. C., Jr., and J. B. Keller
1959. "Elastic wave propagation in homogeneous and inhomogeneous media," *J. Acoust. Soc. Am.*, 31: 694–705.
Knopoff, L., and F. Gilbert
1960. "First motions from seismic sources," *Bull. Seismol. Soc. Am.*, 50: 117–134.
Morse, P. M., and H. Feshbach
1953. "*Methods of theoretical physics*," McGraw-Hill Book Co., New York.
Nakano, H.
1923. "Notes on the nature of the forces which give rise to the earthquake motions," *Seismol. Bull. Central Met. Obs. Japan*, 1: 92–120.
Phinney, R. A.
1964. "Structure of the earth's crust from spectral behavior of long-period body waves," *J. Geophys. Res.*, 69: 2997–3017.
Ritsema, A. R.
1958. "$(i - \Delta)$-curves for bodily seismic waves of any force depths," *Meteorol. and Geophys. Inst. Djakarta, Verhandelingen*, 54: 1–10.
Roller, J. C., and J. H. Healy
1963. "Seismic refraction measurements of crustal structure between Santa Monica Bay and Lake Mead," *J. Geophys. Res.*, 68: 5837–5850.

Seismological Laboratory
California Institute of Technology
Pasadena, California
Division of the Geological Sciences
Contribution No. 1302

Manuscript received October 21, 1964.